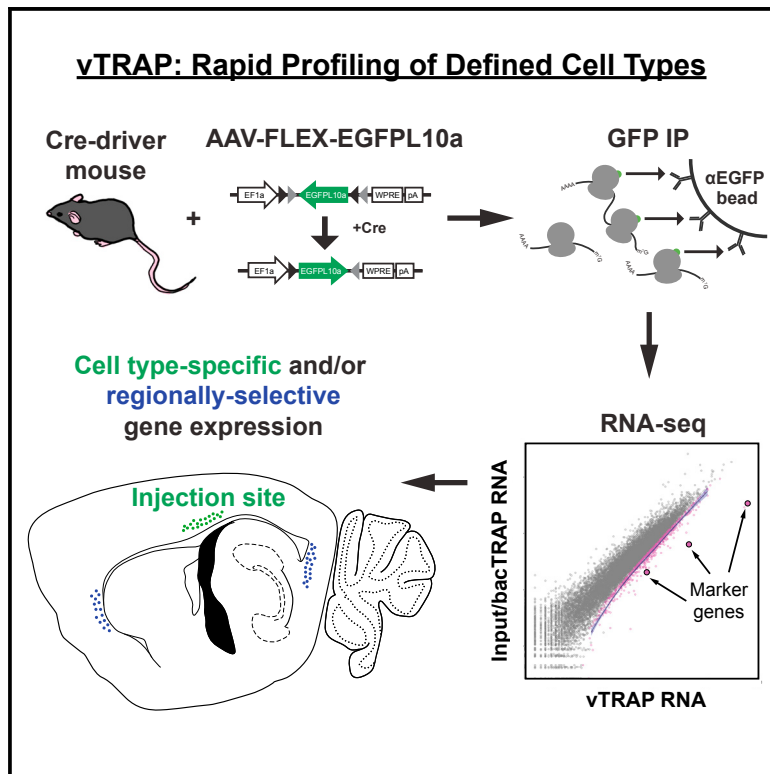


Rapid Molecular Profiling of Defined Cell Types Using Viral TRAP

Graphical Abstract



Authors

Alexander R. Nectow, Maria V. Moya, Mats I. Ekstrand, ..., Jeffrey M. Friedman, Nathaniel Heintz, Eric F. Schmidt

Correspondence

anectow@princeton.edu (A.R.N.), heintz@rockefeller.edu (N.H.), eschmidt@rockefeller.edu (E.F.S.)

In Brief

Nectow et al. describe vTRAP, a technology to purify translating mRNAs from genetically defined cell types in a spatiotemporally restricted fashion. Multiplexing vTRAP with other technologies offers a comprehensive strategy to interrogate the precise role of individual, cell-type-specific genes in neural circuit function.

Highlights

- vTRAP enables rapid, viral-based tagging of translating ribosomes in defined cells
- vTRAP faithfully recapitulates molecular profiles obtained from bacTRAP
- vTRAP can detect regional, cell-type-specific differences in gene expression
- vTRAP was used for comprehensive molecular profiling of LH MCH neurons

Accession Numbers

GSE89737



Rapid Molecular Profiling of Defined Cell Types Using Viral TRAP

Alexander R. Nectow,^{1,2,*} Maria V. Moya,³ Mats I. Ekstrand,¹ Awni Mousa,³ Kelly L. McGuire,³ Caroline E. Sferrazza,³ Bianca C. Field,¹ Gabrielle S. Rabinowitz,⁴ Kirsty Sawicka,⁴ Yupu Liang,⁵ Jeffrey M. Friedman,¹ Nathaniel Heintz,^{3,*} and Eric F. Schmidt^{3,6,*}

¹Laboratory of Molecular Genetics, Howard Hughes Medical Institute, The Rockefeller University, 1230 York Avenue, New York, NY 10065, USA

²Princeton Neuroscience Institute, Princeton University, Lot 20 Washington Road, Princeton, NJ 08544, USA

³Laboratory of Molecular Biology, Howard Hughes Medical Institute, The Rockefeller University, 1230 York Avenue, New York, NY 10065, USA

⁴Laboratory of Molecular Neuro-Oncology, Howard Hughes Medical Institute, The Rockefeller University, 1230 York Avenue, New York, NY 10021, USA

⁵Hospital Informatics, The Rockefeller University, 1230 York Avenue, New York, NY 10021, USA

⁶Lead Contact

*Correspondence: nectow@princeton.edu (A.R.N.), heintz@rockefeller.edu (N.H.), eschmidt@rockefeller.edu (E.F.S.)

<http://dx.doi.org/10.1016/j.celrep.2017.03.048>

SUMMARY

Translational profiling methodologies enable the systematic characterization of cell types in complex tissues, such as the mammalian brain, where neuronal isolation is exceptionally difficult. Here, we report a versatile strategy for profiling CNS cell types in a spatiotemporally restricted fashion by engineering a Cre-dependent adeno-associated virus expressing an EGFP-tagged ribosomal protein (AAV-FLEX-EGFPL10a) to access translating mRNAs by translating ribosome affinity purification (TRAP). We demonstrate the utility of this AAV to target a variety of genetically and anatomically defined neural populations expressing Cre recombinase and illustrate the ability of this viral TRAP (vTRAP) approach to recapitulate the molecular profiles obtained by bacTRAP in corticothalamic neurons across multiple serotypes. Furthermore, spatially restricting adeno-associated virus (AAV) injections enabled the elucidation of regional differences in gene expression within this cell type. Altogether, these results establish the broad applicability of the vTRAP strategy for the molecular dissection of any CNS or peripheral cell type that can be engineered to express Cre.

INTRODUCTION

The characterization of the molecular properties of specific cell types within the brain is essential to better understand CNS function. Differences in the suite of proteins expressed by distinct neuronal populations underlie their unique intrinsic properties, susceptibility to disease, and responses to extrinsic manipulations, such as drugs or trauma. Recent advances in translational

profiling methods have provided direct access to the translating mRNAs of genetically defined cell populations in complex tissues. The translating ribosome affinity purification (TRAP) technique and its variants rely on targeted transgene expression (Doyle et al., 2008; Heiman et al., 2008), connectivity (Ekstrand et al., 2014; Nectow et al., 2015), or even synaptic activity (Knight et al., 2012) to access cell types and overcome the challenges posed by the heterogeneous organization of the CNS. By directing the expression of an EGFP-tagged ribosome protein L10a (EGFPL10a) to defined cell populations, TRAP enables the isolation of cell-type-specific polysome-bound mRNAs from whole-tissue homogenates, avoiding potential adaptations and RNA degradation that can result from lengthier cellular isolation methods (Heiman et al., 2014).

The TRAP approach has been employed to profile translation in dozens of cell types in the mouse CNS (Doyle et al., 2008; Mellén et al., 2012; Nakajima et al., 2014; Schmidt et al., 2012; Shrestha et al., 2015) and visceral organs (Grgic et al., 2014; Zhou et al., 2013) and has been valuable in teasing apart neural circuits underlying complex CNS disease. TRAP has been used to identify a single cortical cell type that mediates antidepressant responses (Schmidt et al., 2012), a population of oxytocin-receptor-expressing interneurons in the prefrontal cortex that modulate sociosexual behavior in females (Nakajima et al., 2014), and cortical cells that integrate stress responses in the context of depressive-like behaviors (Shrestha et al., 2015). It was also applied to identify genes altered in specific neuronal populations in the midbrain (Dougherty et al., 2013) and cerebellum (Mellén et al., 2012) in animal models of neurodevelopmental disorders.

Whereas simple and effective, to date, the application of TRAP to study the mammalian CNS has been dependent on engineered mouse strains for EGFPL10a expression. This has been achieved through the generation of a series of novel bacterial artificial chromosome (BAC) transgenic mouse lines in the “bacTRAP” method (Doyle et al., 2008; Nakajima et al., 2014; Schmidt et al., 2012; Shrestha et al., 2015) or conditional



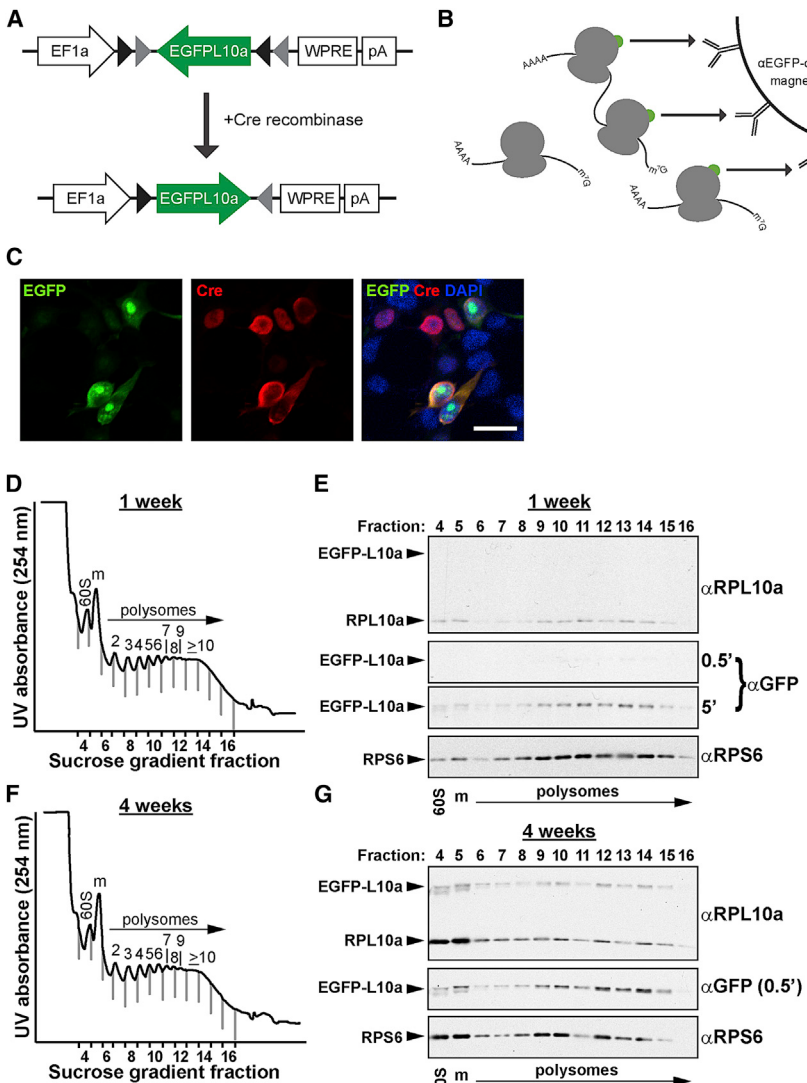


Figure 1. Development and Application of vTRAP Approach

(A) Schematic depicting the design of the Cre-dependent pAAV-FLEX-EGFPL10a vector.

(B) After expression of EGFPL10a transgene in the targeted cell type, EGFP-labeled polysomes are affinity purified to enrich for cell-specific, polysome-bound, translating mRNAs.

(C) Immunofluorescent staining of HEK293T cells co-transfected with pAAV-FLEX-EGFPL10a (green) and pCAG-Cre (red). Nuclei are labeled with DAPI (blue) in right panel. The scale bar represents 20 μm.

(D) Polysome profile plot of sucrose gradient fractions from cortex of Emx1-Cre mice 1 week after AAV-FLEX-EGFPL10a virus injections. Vertical gray lines indicate fraction divisions. Fractions containing the large subunit (60S; fraction no. 4), monosome (m) (no. 5), and polysomes (no. s 6–16) are labeled.

(E) Western blots showing the distribution of the EGFPL10a transgene, endogenous RPL10a, and RPS6 in the sucrose gradient fractions from (D). Short (30 s) and long (5 min) exposures are shown for the anti-GFP blot.

(F) Polysome profile plot of sucrose gradient fractions from cortex of Emx1-Cre mice 4 weeks after AAV-FLEX-EGFPL10a virus injections.

(G) Western blots showing the distribution of the EGFPL10a transgene, endogenous RPL10a, and RPS6 in the sucrose gradient fractions from (F). Anti-GFP blot is from a 30-s exposure.

See also Figure S1.

expression requiring either Cre recombinase (Liu et al., 2014; Sanz et al., 2009; Stanley et al., 2013; Zhou et al., 2013) or tetracycline-controlled transcription (Drane et al., 2014). To expand the utility of the TRAP approach, we generated Cre-dependent adeno-associated viral (AAV) vectors to express EGFPL10a. These vectors enable rapid access to translating mRNAs from any discrete neural population engineered to express Cre recombinase while avoiding the need to cross multiple mouse strains harboring independent alleles and unwanted recombination during development. This viral TRAP (vTRAP) approach can be immediately applied for use with any of the scores of commercially available rodent Cre-driver strains or in a combinatorial manner in other species using Cre-expressing viruses.

Here, we demonstrate the incorporation of virally expressed EGFPL10a into endogenous polysomes and validate the vTRAP approach in a number of readily available Cre-driver mouse strains, interrogating cell types in the brainstem, hypothalamus, and cortex as a proof of concept. With a focus on layer 6 cortico-

thalamic (CThal) cells, we show that vTRAP was able to capture cell-type-specific translational profiles with high fidelity to the traditional bacTRAP approach. Further, the spatially restricted nature of AAV expression revealed the utility of the vTRAP approach for more localized molecular profiling within neural

structures. Taken together, the current work provides a strategy for the rapid and highly efficient targeting of translating ribosomes in a cell-type-specific, anatomically restricted fashion using viral-mediated gene transfer.

RESULTS

Generation and Validation of AAV-FLEX-EGFPL10a

To develop a viral construct that can be used for translational profiling, EGFPL10a was cloned in the reverse orientation into the Cre-dependent pAAV-EF1a-DIO-ChR2-mCherry plasmid, replacing ChR2-mCherry. The flanking loxP and lox2272 sites were left intact, resulting in a virus that had a “double-floxed” inverted open reading frame, or “FLEX switch” (Atasoy et al., 2008), to allow for cell-type-specific expression of the EGFPL10a fusion protein. This construct is hereafter referred to as pAAV-FLEX-EGFPL10a (Figure 1A). In the presence of Cre recombinase, EGFPL10a is reverted back to the “expressed” forward

orientation, allowing for conditional expression of a functional protein. Once incorporated into the large ribosomal subunit, the EGFPL10a protein allows for cell-type-specific polysome immunoprecipitation using the TRAP method (Figure 1B). To confirm Cre-dependent expression of the EGFPL10a construct, we co-transfected HEK293T cells with pAAV-FLEX-EGFPL10a and pCAG-Cre-Myc. Immunofluorescent staining for EGFP and c-Myc revealed that expression of the EGFPL10a transgene was restricted only to cells co-stained with anti-Myc and thus contained the Cre plasmid (Figure 1C).

To demonstrate integration of the EGFPL10a construct into translating ribosomes *in vivo*, pAAV-FLEX-EGFPL10a was packaged into AAV. The viral vectors were then injected into the cerebral cortex of Emx1-IRES-Cre mice, which express Cre recombinase in most pyramidal cells throughout the neocortex (Gorski et al., 2002). We looked for incorporation of the EGFPL10a transgene into polysomes at 1 week and 4 weeks following virus injections. Polysomes were purified by linear sucrose gradient fractionation of cytosolic lysates from AAV-injected cortex (Figures 1D–1G). Western blots of trichloroacetic acid (TCA)-precipitated sucrose gradient fractions revealed that the distribution of EGFPL10a overlapped significantly with endogenous RPL10a as well as RPS6 ribosome subunits, demonstrating that the transgene was inserted into functional polysomes (Figures 1E, 1G, and S1). Immunoblots using anti-GFP antibody showed that, even after only 1 week, EGFPL10a could be detected in polysome fractions (Figures 1E and S1A). However, levels of EGFPL10a protein were substantially higher 4 weeks after virus injection (Figures 1G and S1B), likely reflecting the timeline needed for maximal AAV expression (Kaspar et al., 2002) and the 2- to 3.5-week turnover rate of ribosomal proteins in the mouse brain (Price et al., 2010). Taken together, these results demonstrate the ability of AAV-FLEX-EGFPL10a to drive Cre-dependent expression of EGFPL10a to label polysomes *in vivo*.

Using AAV-FLEX-EGFPL10a to Target Genetically Defined Neuronal Populations *In Vivo*

We next set out to validate functional expression of AAV-FLEX-EGFPL10a in various neural populations throughout the brain. We used existing Cre recombinase transgenic lines to drive expression specifically in dorsal thalamus, cortex, and midbrain (Figures 2A–2C). Anti-GFP immunostaining revealed bright puncta within the nucleolus (Figure 2B), the site of ribosomal biogenesis, and is consistent with transgenic EGFPL10a expression in bacTRAP mice.

To confirm functional integration of EGFPL10a, we performed anti-EGFP immunoprecipitations (IPs) to purify polysomes from specific populations of monoaminergic neurons in the brainstem. We focused on two well-characterized populations each with a set of known cell-specific marker genes: dopaminergic (DA) neurons of the ventral tegmental area (VTA) and serotonergic (5-HT) neurons of the dorsal raphe nucleus (DRN). AAV-FLEX-EGFPL10a was injected into the VTA of DAT-Cre and the DRN of SERT-Cre mice. IPs from each region resulted in substantial RNA yields (average of >9 ng total RNA per IP; data not shown), suggesting that EGFPL10a protein was incorporated into translating ribosomes in each of these cell types. qRT-PCR showed significant specificity for known marker genes for

each cell type in the IPs from VTA DA and DRN 5-HT neurons (Figure 2D). Dopaminergic marker genes *Slc6a3* (16.1-fold) and *Th* (25.6-fold) were significantly enriched in DA neurons, whereas serotonergic marker genes *Slc6a4* (267.6-fold) and *Fev* (182.6-fold) were significantly enriched in 5-HT neurons. In contrast, there was no significant difference in *Slc32a1* enrichment, which is known to be depleted from both populations. Lastly, AAV-FLEX-EGFPL10a injection into wild-type mice resulted in negligible RNA yields, demonstrating the dependence of this virus on the presence of Cre for detectable EGFPL10a expression (Figure S2A). Together, these data demonstrate proper conditional expression and functional integration of the AAV-expressed EGFPL10a transgene *in vivo*.

Molecular Profiling of Lateral Hypothalamic MCH Neurons

To demonstrate the utility of the vTRAP approach, we characterized the molecular properties of a less well-studied population of neurons in the lateral hypothalamus (LH). The LH is known to be a critical node in controlling survival-related behaviors, such as food intake. Melanin-concentrating hormone (MCH) neurons comprise a significant population within the LH and are known to regulate feeding behavior and sucrose preference (Domingos et al., 2013; Shimada et al., 1998). The sparse distribution of MCH neurons in LH has hindered molecular profiling in the past, making them ideal for comprehensive molecular profiling with vTRAP. We injected AAV-FLEX-EGFPL10a into the LH of *Pmch*-Cre mice and confirmed cell-type-specific expression of EGFPL10a in MCH neurons (Figure 3A). qRT-PCR on vTRAP RNA showed significant enrichment for the cell type marker *Pmch* (77.7-fold), as well as *Cartpt* (15.3-fold) and *Tacr3* (12.1-fold), two genes co-expressed in MCH neurons (Crozier et al., 2010; Knight et al., 2012; Figure 3B). We also found significant depletion of *Agrp*, a marker for the arcuate nucleus (2.4-fold; Figure 3B).

High-throughput RNA sequencing (RNA-seq) of vTRAP RNA was performed for comprehensive molecular profiling of MCH neurons (Figure 3C). Differential analysis identified 1,761 genes enriched in the IP over LH input. Notably, the most significantly enriched gene in the entire dataset was *Pmch* (99-fold), the driver gene for MCH neurons. Additionally, *Cartpt* (23.7-fold) and *Tacr3* (8.2-fold) were among the top 20 most significantly enriched genes (Figure 3D). A direct comparison of vTRAP with TRAP done on LH from *Pmch*-Cre mice crossed to the Cre-dependent EGFPL10a reporter line, *Rosa26^{fsTRAP}* (Zhou et al., 2013), showed substantial reproducibility with regard to control genes (*Pmch*, *Cartpt*, *Tacr3*, *Agrp*, and *Anxa1*) and MCH markers identified by vTRAP (*Crhbp*, *Dmrtb1*, and *Mup6*; Figures S2B and S2C), further validating the efficacy of the viral approach. An earlier study using the Retro-TRAP approach (Ekstrand et al., 2014) identified a number of genes expressed in hypothalamic cells with projections to the nucleus accumbens (NAc) that included but were not restricted to MCH neurons. Comparative analysis of MCH vTRAP results with NAc Retro-TRAP data (Figure 3E) identified a number of transcripts that were significantly enriched in both datasets, including *Crhbp* (6.9-fold), *Dmrtb1* (12.2-fold), and *Mup6* (77.1-fold; Figure 3F). However, we found *Anxa1* ($p < 0.01$; 6.4-fold differential enrichment), a gene specific to midbrain dopaminergic projections to striatum (Ekstrand et al.,

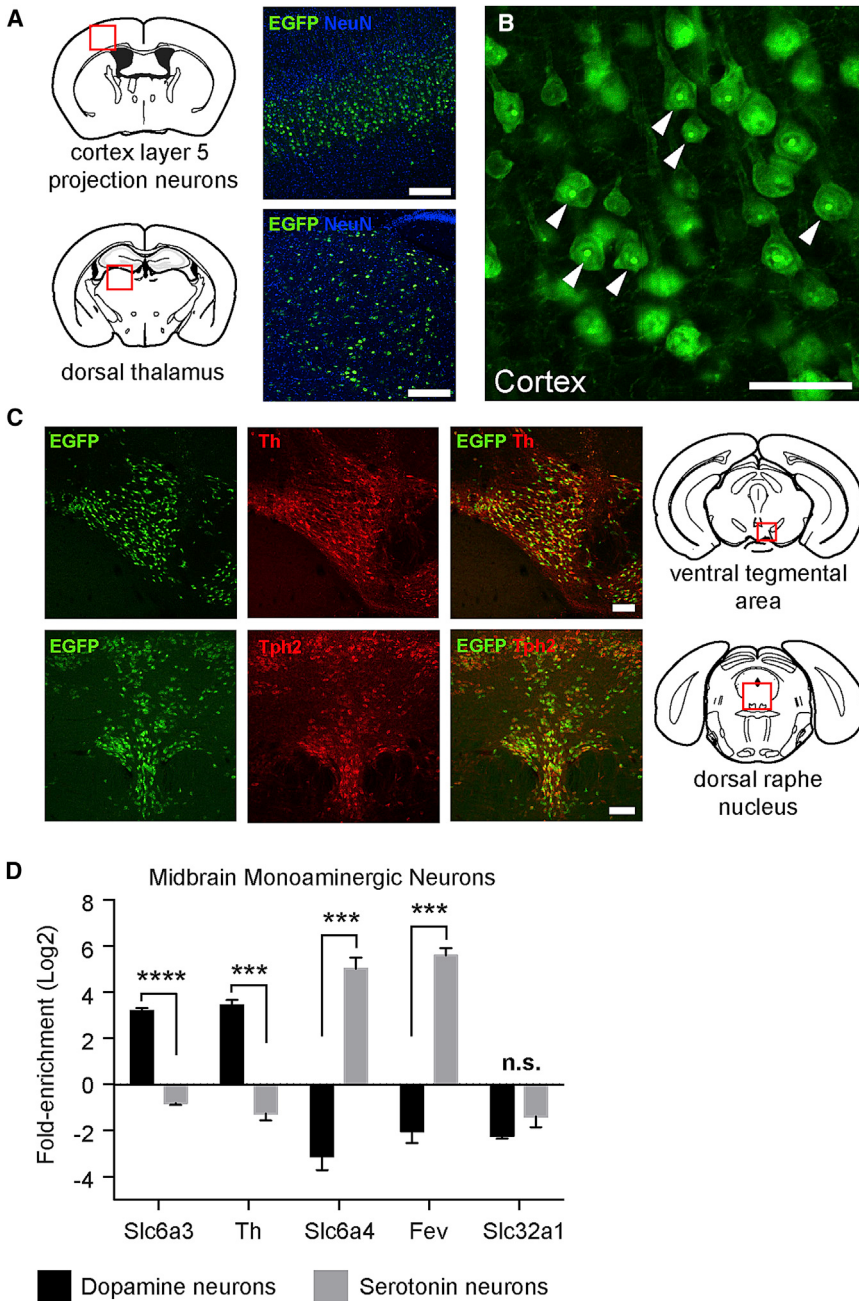


Figure 2. In Vivo Application of vTRAP in Defined Cell Populations

(A) EGFP10a expression in cortex of Tlx3-Cre (top) or thalamus of Slc17a6-Cre (bottom) mice injected with AAV-FLEX-EGFPL10a. Schematics of coronal sections, adapted from Franklin and Paxinos (2008), depicting the relative location of the images (red boxes) are shown on the left, and anti-GFP (green) and NeuN (blue) immunofluorescence from tiled scans of cortex are shown on the right. The scale bars represent 200 μ m.

(B) High-magnification image of anti-GFP immunofluorescence from a tiled scan of cortex of the Tlx3-Cre mouse from (A). Arrowheads indicate GFP labeling in the nucleolus. The scale bar represents 50 μ m.

(C) Co-localization between EGFP10a (EGFP, green) and tyrosine hydroxylase (Th, red) in the VTA of a DAT-Cre mouse (top panels) and EGFP10a (EGFP, green) and tryptophan hydroxylase 2 (Tph2, red) in the DRN of a SERT-Cre mouse (bottom panels). Schematics at left depict the relative location of the images (red boxes). The scale bars represent 100 μ m.

(D) qRT-PCR quantification (mean \pm SEM) of the expression of marker genes for DA (*Slc6a3* and *Th*), 5-HT (*Slc6a4* and *Fev*), or GABA (*Slc32a1*) neurons in VTA (black bars) or DRN (gray bars).

*** $p < 0.001$; **** $p < 0.0001$.

2014), and *Pmch* (15-fold difference; $p < 0.0001$) were significantly differentially expressed between these datasets, reflecting the ability of vTRAP to overcome the heterogeneity of projections to the NAc (Figure 3F). These results suggest that the combined use of vTRAP and Retro-TRAP data can allow comprehensive projection- and cell-type-specific profiling of neural circuits.

vTRAP from Multiple AAV Serotypes Enriches for Cell-Specific Markers in Layer 6 Corticothalamic Neurons

The efficacy of infection of recombinant AAV vectors for different classes of cells is dependent on the nature of the capsid proteins

that coat the outer surface of the virus particles. To test whether we could detect noticeable differences in the ability of vTRAP to enrich for cell-type-specific genes between discrete AAV serotypes, we created pAAV-FLEX-EGFPL10a vectors packaged using three separate capsids commonly used to target neurons in the CNS: AAV2; AAV5; and AAV9 (Aschauer et al., 2013). For these experiments, we examined corticothalamic (CThal) projection neurons that reside in layer 6 of the neocortex because this cell population has been targeted by distinct BAC transgenic lines that express either Cre recombinase (Gong et al., 2007) or EGFPL10a (Doyle et al., 2008). A triple cross of Ntsr1-bacTRAP, Ntsr1-Cre, and Rosa26^{tdTomato} reporter mice revealed a

nearly complete overlap of EGFPL10a expression and Cre activity in L6 cells in cortex (Figures S3A and S3B), validating a direct comparison of these lines.

AAV vectors were injected into sensorimotor areas of neocortex of Ntsr1-Cre mice. EGFPL10a expression was detected throughout layer 6 of Ntsr1-bacTRAP mice and in layer 6 at the injection site in the Ntsr1-Cre mice (Figure 4A). Viral-mediated expression of EGFPL10a was relatively higher than transgenic expression in the bacTRAP mice, likely reflecting the constitutive nature of the AAV's strong EF1a promoter after Cre-mediated recombination. Remarkably, viral expression in

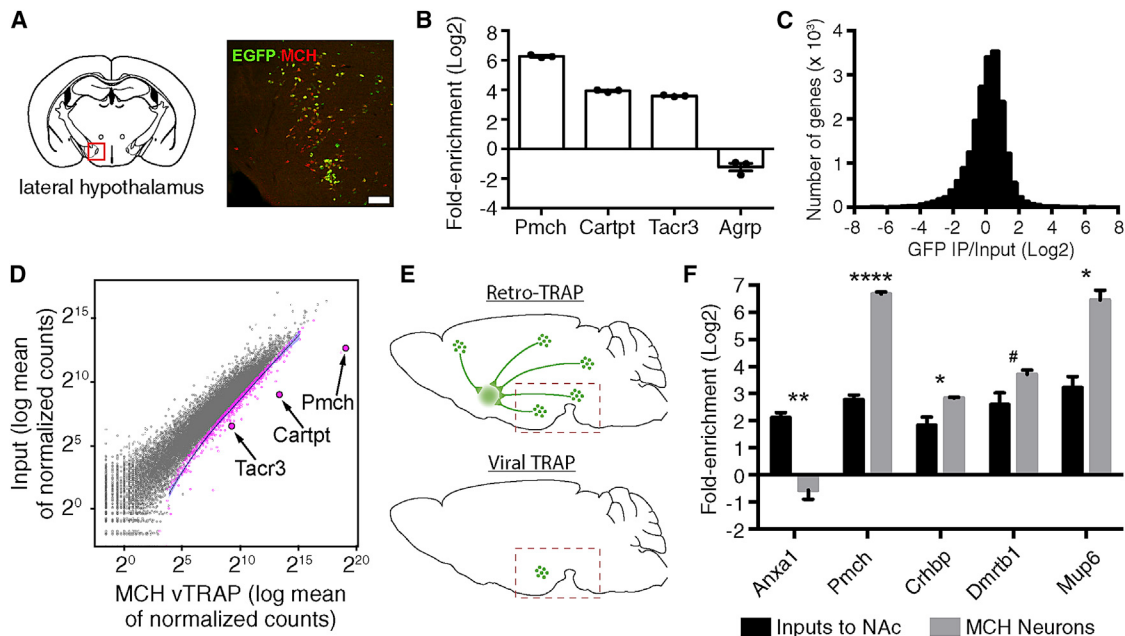


Figure 3. Molecular Profiling of Lateral Hypothalamic MCH Neurons

(A) Colocalization between EGFP and MCH. Red box indicates region of interest. The scale bar represents 200 μm.
 (B) qRT-PCR (mean ± SEM) of cell type marker genes (*Pmch*, *Cartpt*, and *Tacr3*) and a non-MCH neuron marker gene (*Agrp*) after IPs from the hypothalamus. $p < 0.01$ for *Pmch* and *Cartpt* and $p < 0.05$ for *Tacr3* and *Agrp*.
 (C) Histogram plotting RNA-seq data from MCH neuron vTRAP, displaying number of genes as a function of fold enrichment.
 (D) Scatterplot of RNA-seq results from MCH vTRAP showing normalized counts from IP (x axis) and hypothalamus input (y axis). Gray dots represent individual genes (pink are significantly enriched in the IP). MCH neuron markers (*Pmch*, *Cartpt*, and *Tacr3*) are highlighted. Blue line is the best fit curve for all enriched genes.
 (E) Schemata for Retro-TRAP (top) and vTRAP (bottom). For Retro-TRAP, a retrograde tracing virus, CAV-GFP is injected into the NAc of SYN-NBL10 transgenic mice, enabling profiling of NAc inputs from midbrain and hypothalamus. For vTRAP, Cre-dependent AAV-FLEX-EGFPL10a is injected into the LH of Pmch-Cre transgenic mice. Dashed box shows approximate dissection site.
 (F) RNA-seq comparison (fragments per kilobase per million mapped reads [FPKM] mean ± SEM) of genes enriched in both Retro-TRAP (inputs to NAc; data from Ekstrand et al., 2014) and MCH vTRAP (MCH neurons) datasets. * $p < 0.05$; ** $p < 0.01$; *** $p < 0.0001$; # $p = 0.052$.

See also Figure S2.

Ntsr1-Cre mice led to clear EGFP signal in distal CThal axons and terminal fields in the thalamus (Figures S3C and S3D). This implies a utility for vTRAP to isolate locally translated transcripts in axons, providing a straightforward strategy for profiling translation from anatomically separated subcellular compartments.

To establish translational profiles of the CThal cells, we isolated polysome-bound mRNA by TRAP from cortex of *Ntsr1*-bacTRAP mice and *Ntsr1*-Cre mice injected with each of the AAV serotypes. Global differences in gene expression between TRAP IP mRNA (IP) and whole cortex (input) were analyzed by RNA-seq. Despite the inherent variability of virus spread, infection rate, and expression levels between individual virus injections, the biological reproducibility for all vTRAP samples was extremely high ($r^2 \sim 0.97\text{--}0.98$ for all groups; Figure S4A). In each case, greater than 600 genes were shown to be enriched in the *Ntsr1* cell population (Figures 4B and S4B). Two layer 6 markers, *Foxp2* and *Syt6*, were highly enriched in the sequencing data from the bacTRAP and vTRAP IPs using AAV5 and AAV9 compared to inputs, whereas markers for oligodendrocytes (*Mal*) and for cortical layer 5 neurons (*Tmem200a*) were depleted (Figures 4B, 4C, and S4C). qRT-PCR confirmed

the RNA-seq results, showing that levels of enrichment of *Foxp2* and *Syt6* in TRAP IP RNA and depletion of *Mal* and *Tmem200a* were similar between the bacTRAP, AAV5 vTRAP, and AAV9 vTRAP samples (Figure 4D). Surprisingly, whereas *Ntsr1*, *Foxp2*, and *Syt6* were significantly enriched in AAV2 vTRAP IPs, the degree of enrichment was significantly less than the other groups (Figures 4B and 4D).

Translational Profiles from vTRAP Benchmarked against bacTRAP

TRAP-seq data from the MCH LH and CThal neurons clearly demonstrate that the vTRAP approach can enrich for cell-type-specific marker genes similar to transgenic TRAP methods. To ask how well vTRAP translational profiles correlate with those from bacTRAP, we generated a list of genes specific to the CThal population. We applied the “specificity index” (SI) algorithm, a comparative rank-order approach that identifies genes that are unique to each dataset (e.g., cell type) in a given analysis (Dougherty et al., 2010) to bacTRAP data from six neuronal and non-neuronal cortical cell types. In addition to CThal cells, our analysis included layer 5a corticostriatal cells, layer

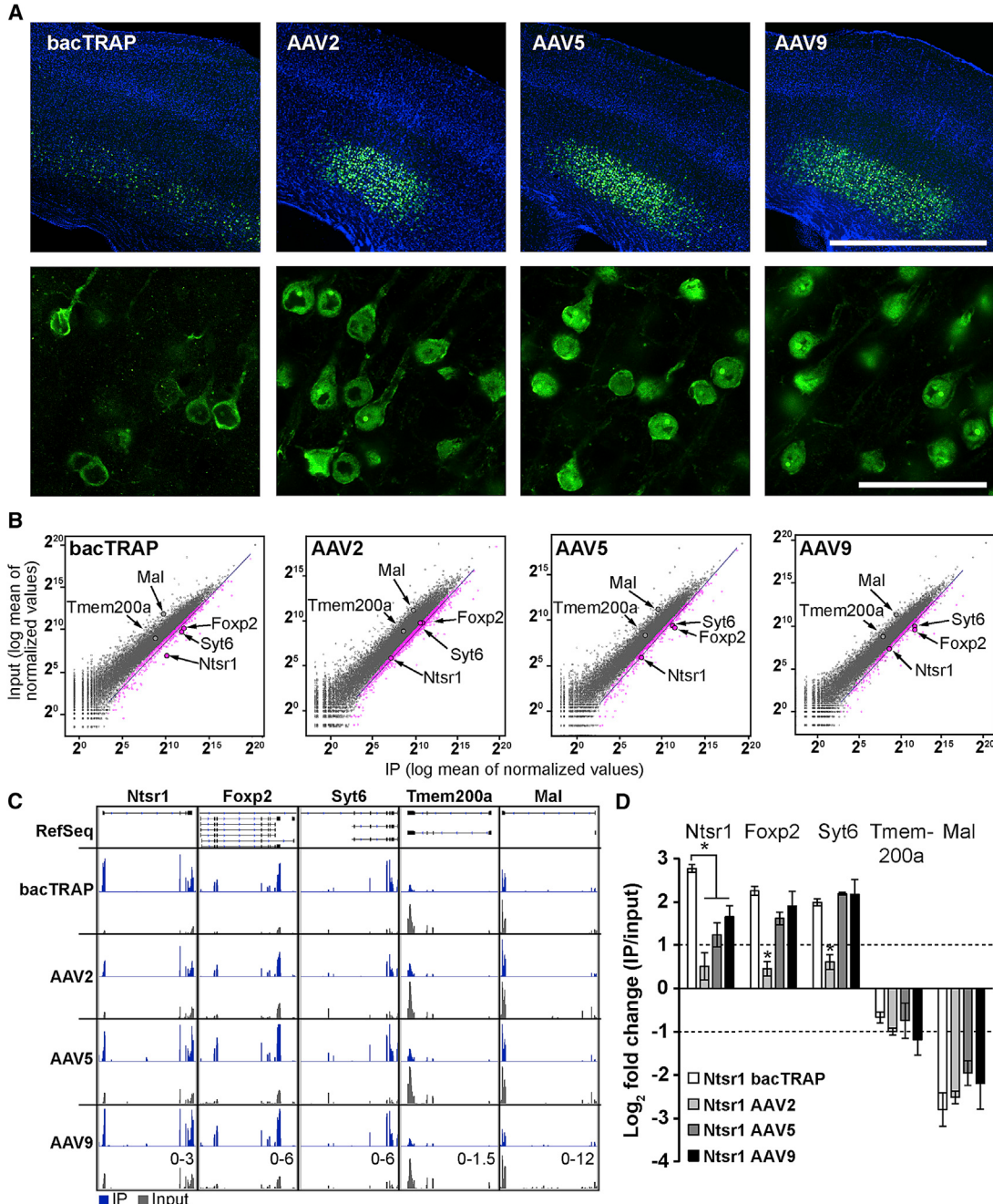


Figure 4. vTRAP Molecular Phenotyping of Layer 6 CThal Cells Using Three AAV Serotypes

(A) Low- (top) and high (bottom)-magnification images showing EGFP10a expression restricted to layer 6 in cortex of Ntsr1-bacTRAP (far left) and Ntsr1-Cre mice injected with vTRAP vectors. Anti-EGFP is shown in green, and DAPI is shown in blue. Low-magnification images were taken from composites of tiled scans of coronal brain slices. The scale bars represent 1 mm (top) and 50 μ m (bottom).

(B) Scatterplots of TRAP-seq results showing normalized counts from IP (x axis) and whole-cortex input (y axis) from Ntsr1-bacTRAP (far left) and Ntsr1-Cre mice injected with vTRAP vectors (right). Dots represent individual genes (pink are significantly enriched in IP). The driver gene (*Ntsr1*) and layer 6 markers (*Foxp2* and *Syt6*) are labeled. Blue line is the best fit curve for enriched genes.

(C) Visualization of reads from TRAP-seq datasets shown in (B) mapped to the genomic locus of three cell-type-specific marker genes (*Ntsr1*, *Syt6*, and *Foxp2*), a cortical layer 5 gene (*Tmem200a*), and a glial gene (*Mal*). TRAP IP samples are colored blue, and their corresponding inputs are shown in gray. RefSeq gene structure is illustrated in black at top (exons are vertical bars). The scale of the y axis is shown at bottom right for each gene.

(D) qRT-PCR quantification (mean \pm SEM) of the expression of control genes shown in (C) for bacTRAP and vTRAP samples compared to whole-cortex input. Positive values indicate enrichment in the IP. Dotted lines represent 2-fold enrichment in either direction. * $p < 0.05$.

See also Figure S3.

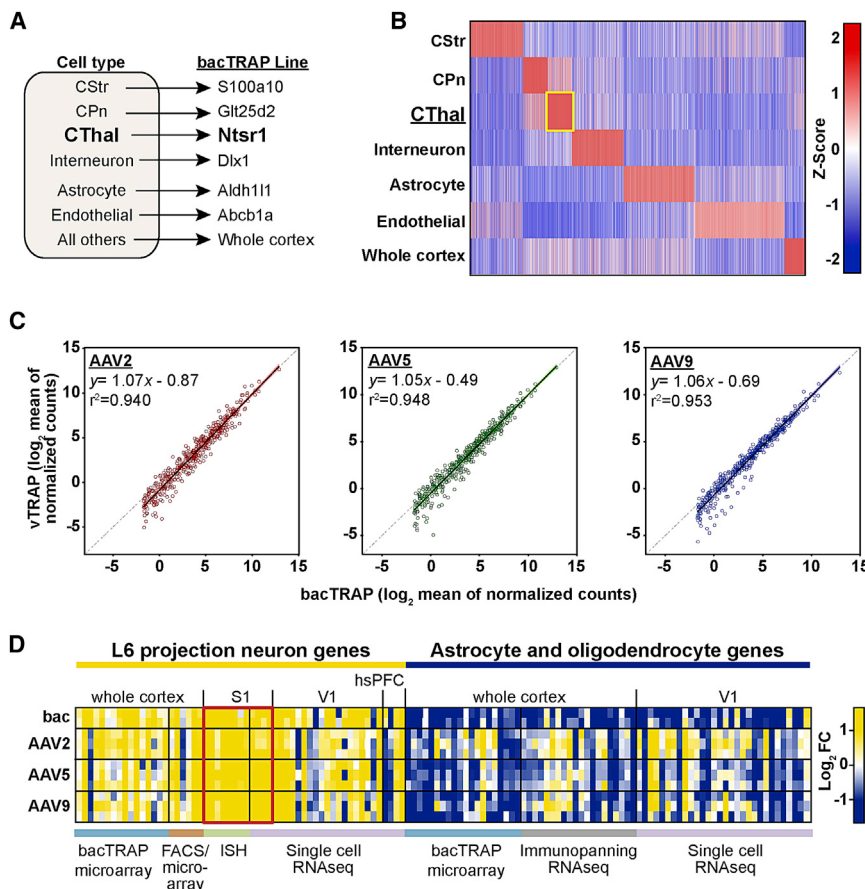


Figure 5. The Enrichment of Cell-Type-Specific Genes Is Highly Correlated between vTRAP and bacTRAP Approaches

(A) Schematic depicting the datasets used to target specific cell populations in the cerebral cortex. CPn, corticopontine; CStr, corticostratial; CThal, corticothalamic.

(B) Heatmap of cell-specific genes (horizontal axis) from bacTRAP lines representing six distinct cell populations and whole tissue from the cerebral cortex. Color is based on the normalized expression for each cell type, and only genes with a p value (p_{SI}) < 0.05 are shown. Yellow box indicates the CThal (Ntsr1-bacTRAP)-specific genes.

(C) Scatterplots comparing the expression of CThal-specific genes from (B) between Ntsr1 bacTRAP (x axis in each) and Ntsr1 vTRAP (y axis) vectors. The linear equation and coefficient of determination (r^2) are shown at the top of each graph, and the best fit curve for each dataset is shown as a solid line.

(D) Heatmap showing enrichment (TRAP IP/input) of marker genes for L6 projection neurons (left) or glial cells (right) identified by a variety of experimental approaches. Rows are individual replicates from bacTRAP (“bac”) and vTRAP datasets. The cortical region analyzed in each study is labeled on top, and color-coded bars at bottom indicate the cell-type isolation method. Red box emphasizes genes identified from S1, which overlaps with the vTRAP virus injection site. hsPFC, human prefrontal cortex; S1, mouse primary somatosensory; V1, mouse primary visual. See also Tables S1, S2, and S3 and Figures S4 and S5.

5b corticopontine cells, interneurons, astrocytes, endothelial cells, and whole cortex, which included all other cell types (Figure 5A; Table S1). All bacTRAP mouse strains targeting these cell populations have been described elsewhere (Doyle et al., 2008; Nakajima et al., 2014; Schmidt et al., 2012) except for the endothelial cell-specific Abcb1a-bacTRAP line (see Figures S3E and S3F and Supplemental Information).

The SI algorithm identified 428 genes with $p_{SI} < 0.05$ for the Ntsr1 CThal population (Figure 5B; Table S2). A direct comparison of sequencing results from vTRAP and bacTRAP revealed an extremely high correlation in the expression of these CThal-specific genes between both methods for each serotype (Figure 5C). The coefficient of determination (r^2) for each comparison was extremely high (≥ 0.940), and the slope of the best fit curves were all close to 1.0 (Figure 5C). There was a slight bias toward the bacTRAP dataset in all three vTRAP conditions (y intercept ranged from -0.49 to -0.87), likely due to vTRAP sampling only a subset of Ntsr1-expressing cells located near the injection site. The levels of expression of IP-enriched genes were also very similar between these methods (Figure S5C). These results demonstrate the ability of the viral approach to obtain cell-specific translational profiles with high fidelity to bacTRAP.

To assess the utility of vTRAP in the context of other cell-type-specific profiling methods, we compiled a list of layer 6 projection neuron markers in various regions of cortex identified

by sorting retrogradely labeled cells (Galazo et al., 2016), in situ hybridization (ISH) (Sorensen et al., 2015), bacTRAP (Doyle et al., 2008), and single-cell RNA-seq from mouse (Tasic et al., 2016; Zeisel et al., 2015) or human (Lake et al., 2016) cortex (Table S3). The overwhelming majority of these genes were significantly enriched in the vTRAP IPs, including all of the genes identified in studies focused on primary somatosensory cortex (S1), which overlaps with our virus injection site (Figure 4D). In contrast, most astrocyte and oligodendrocyte genes identified by bacTRAP (Doyle et al., 2008), immunopanning (Zhang et al., 2014), or single-cell RNA-seq (Tasic et al., 2016) were depleted in vTRAP IPs (Figure 4D, right). The sensitivity of vTRAP compares favorably to single-cell RNA-seq with over 92% of the top 1,000 genes identified in single-cell datasets from three overlapping populations of L6 cells being detected in Ntsr1 cells by vTRAP (Figures S5A and S5B). Conversely, many low-expressed genes (reads per kilobase per million mapped reads [RPKM] < 10) significantly enriched in vTRAP IPs were not detected in individual single-cell RNA-seq datasets (Figures S5D and S5E).

Direct Comparison of bacTRAP and vTRAP Reveals Regionally Expressed Genes

Because the AAV injections targeted a spatially restricted population of Ntsr1-expressing cells compared to the widely

distributed bacTRAP-labeled cells, we asked whether a comparison of these approaches could identify anatomically restricted genes that may be used to define subregions of cortex. We created lists of “bacTRAP-specific” and “vTRAP-specific” genes, defined as the union of those differentially expressed between bacTRAP and vTRAP AAV9 IP samples and enriched in the IP over input for each approach (Figure S6A). Forty-three bacTRAP-specific genes (Figure 6A, blue circles) and 50 vTRAP-specific genes (Figure 6A, orange circles) were identified. These genes accounted for only a minority of the IP-enriched transcripts in each approach (6.7% for bacTRAP and 8.3% for vTRAP), reflecting the high correlation between the techniques.

ISH data from the Allen Mouse Brain Atlas (Lein et al., 2007) were utilized to examine the distribution of bacTRAP-specific or vTRAP-specific genes in the cortex (see [Supplemental Experimental Procedures](#)). Whereas about one-third of the genes in each dataset were expressed throughout the cortex (Figure 6B; “widespread”), the expression patterns of 37% (16) of the bacTRAP-specific genes were restricted to regions of the cortex that did not overlap with the site of the vTRAP AAV injections (Figure 6B; “regional”). These included genes such as *Col23a1*, which was expressed in rostralateral cortex, and *Cbln1*, *Nnat*, and *L6g6e*, which were found at extreme rostral and caudal cortical sites (Figures 6C, S6C, and S6D). ISH for endogenous *Ntsr1* revealed high expression in entorhinal cortex in addition to layer 6 CThal cells, and anti-GFP immunostaining confirmed this pattern was recapitulated in the *Ntsr1*-bacTRAP mice (Figure 6D). Indeed, entorhinal cortex-specific genes *Mum111*, *Fam70b*, *Lef1*, *Cldn1*, *Cbln4*, and *Pth2r* were not detected by vTRAP but were all present on the bacTRAP-specific list (Figures 6E, S6C, and S6D). Regionally expressed genes accounted for the majority of those with the highest fold change in bacTRAP over vTRAP (red circles in Figure 6A), including pSI-identified CThal genes (Figure S6B). In fact, 31 of the 43 (72%) bacTRAP-specific genes were also significantly enriched when bacTRAP was compared to AAV2 and AAV5 vTRAP data, including 11 of the 16 regional genes, demonstrating remarkable consistency between AAV serotypes. Quantification by qRT-PCR confirmed these differences in expression between bacTRAP and vTRAP with *Cbln1*, *Cbln4*, *Cldn1*, and *Nnat*, all significantly enriched in bacTRAP IP and significantly depleted in vTRAP IP for each of the AAV vectors used ($p < 0.05$ for all genes in each group), whereas *Pth2r* was significant for AAV9, the dataset used to generate the vTRAP-specific list (Figure 6G). Failure to identify vTRAP-specific regional genes may be due to cell-specific genes being enriched in both datasets due to the overlap in expression between bacTRAP and vTRAP, whereas bacTRAP-specific regional genes are depleted from vTRAP data, leading to high differential expression.

DISCUSSION

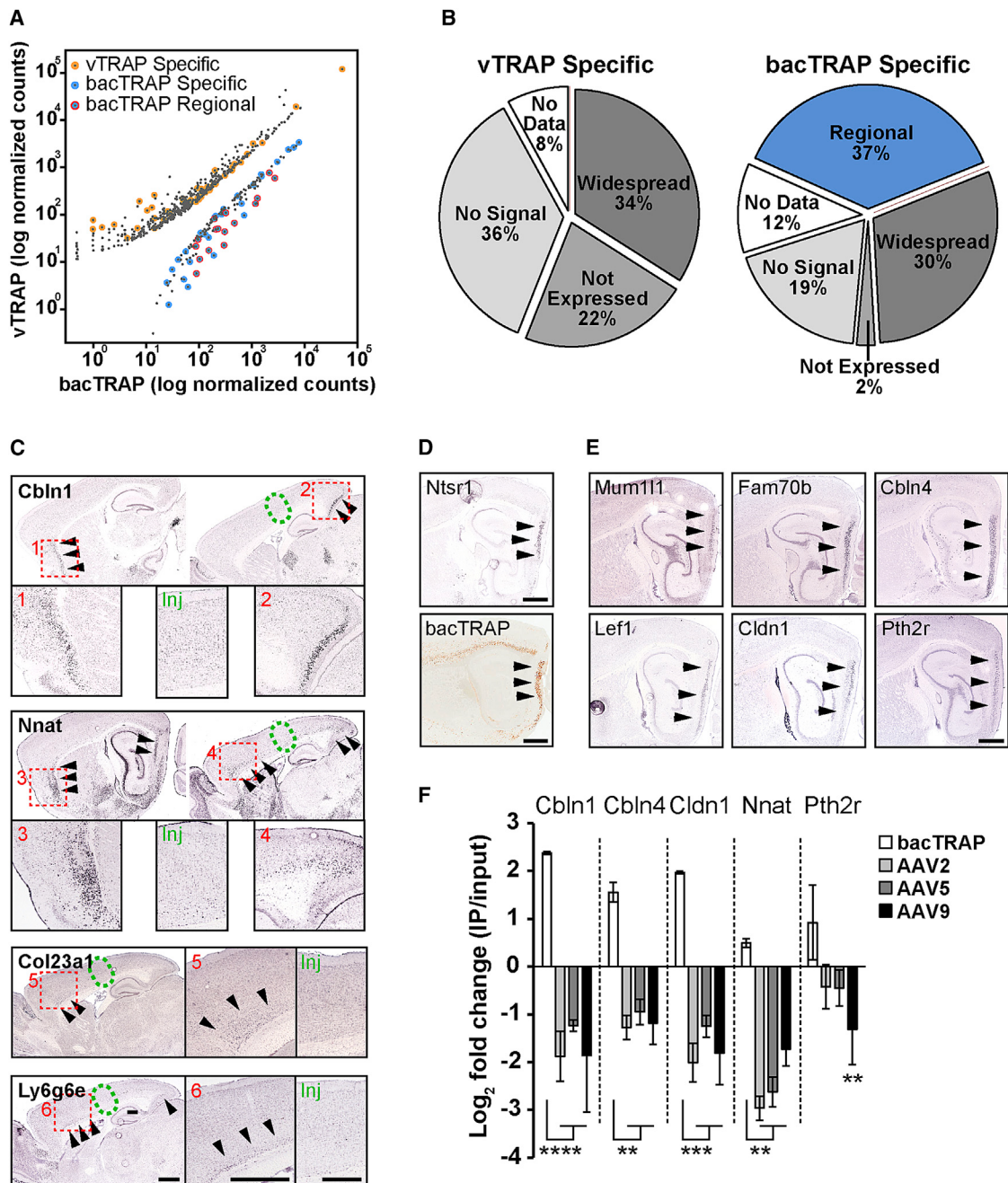
The TRAP technique has traditionally relied on engineered mouse strains to target the EGFPL10a transgene to cell types of interest. In the current work, we extend the TRAP method to take advantage of viral-mediated gene transfer, enabling rapid

and anatomically restricted molecular profiling of any cell type engineered to express Cre recombinase. The broad availability of Cre-driver lines (Gerfen et al., 2013; Gong et al., 2007; Madsen et al., 2010; Taniguchi et al., 2011) allows the viral TRAP strategy to be applied immediately to myriad cell types without the need to generate novel transgenic strains or cross existing lines to Cre-dependent reporters. AAV-mediated overexpression of the TRAP transgene also enables high-quality translational profiling data to be generated as early as 3 weeks following virus injection, allowing for substantial temporal flexibility when designing experiments. Further, viral delivery of the EGFPL10a transgene into adult mouse tissue overcomes the possibility of off-target recombination due to transient expression of Cre in unwanted cell types during development (Lam et al., 2011; Padilla et al., 2010). Cre driver lines that rely on promoters with temporally dynamic expression patterns (Sanz et al., 2009) impose a significant limitation on the utility of Cre-dependent TRAP and RiboTag reporter strains.

The AAV-mediated strategy expands the utility of TRAP to other mammalian species that have historically proven to be genetically intractable. For example, the AAV-FLEX-EGFPL10a vector can immediately be used with the growing number of Cre-expressing rat strains (Witten et al., 2011) or in combination with Cre-expressing viruses in non-transgenic animals, such as monkeys (Oguchi et al., 2015). Projection-specific profiling can also be achieved with vTRAP by combining AAV-FLEX-EGFPL10a with viruses that transduce neurons in a retrograde fashion, such as rabies or canine adenovirus (Schwarz et al., 2015).

Cell-type-specific expression of AAV-FLEX-EGFPL10a in cortex, thalamus, brainstem, and hypothalamus demonstrates the utility of vTRAP to profile a variety of cell types throughout the brain. It also presents a strategy to quickly characterize unknown cell populations labeled with Cre. A simple vTRAP experiment followed by qPCR for selected target genes can easily ascertain neuronal or non-neuronal identity, the neurotransmitter profile (e.g., excitatory, inhibitory, or modulatory), receptor composition, and other properties of the cells without the need for detailed anatomical or electrophysiological investigation. The GENSAT library of Cre-driver mice alone contains a number of strains that express Cre in scattered, morphologically ambiguous cells in areas such as the cortex, hypothalamus, hippocampus, midbrain, and brainstem. These may represent uncharacterized cell populations or known cell types that were not genetically labeled previously.

The observation of EGFPL10a expression in distal axons of projection neurons following AAV-FLEX-EGFPL10a injections presents vTRAP as an intriguing approach to profile axon-specific transcripts *in vivo*. Translational profiling of axonal mRNA (“axon-TRAP”) has previously been achieved in the developing retinotectal system by transplanting transgenic tissue into wild-type animals (Yoon et al., 2012) or relying on very specific transgenic mouse lines with high levels of transgene expression (Shigeoka et al., 2016). The spatial and temporal control of virus injections overcomes these technical hurdles and precludes a reliance on highly restricted Cre driver lines, allowing vTRAP to be exploited for axon profiling of a wider selection of cell types and even across

**Figure 6. Differential Expression between vTRAP and bacTRAP Reveals Regionally Expressed Genes**

(A) Scatterplot of the expression of genes differentially expressed between bacTRAP (x axis) and vTRAP with the AAV9 vector (y axis) IP samples. Yellow circles are vTRAP-specific genes, and blue circles are bacTRAP specific. Genes with regional expression outside of the site of AAV injection are circled in red.

(B) Pie charts of the quantification of expression pattern scores of genes significantly enriched in vTRAP IP versus input and vTRAP over bacTRAP ("vTRAP specific") or bacTRAP IP versus input and bacTRAP over vTRAP ("bacTRAP specific").

(C) ISH in cortex of selected bacTRAP-specific genes with regional expression. Green ovals specify the relative injection site of vTRAP vectors, and arrowheads identify regions with high expression. Insets show higher magnification of boxed areas 1–6 or the relative AAV injection site (Inj) for each gene.

(D) ISH for endogenous *Ntsr1* (top) and anti-EGFP immunolabeling of *Ntsr1*-bacTRAP mouse brain (bottom) showing expression in entorhinal cortex (arrowheads).

(E) ISH of selected "regional" bacTRAP-specific genes with high expression in the entorhinal cortex (arrowheads). All *in situ* hybridization images in (C)–(E) are © 2007 Allen Institute for Brain Science. Allen Mouse Brain Atlas. Available from: <http://www.mouse.brain-map.org>. See Table S4 for datasets used.

(F) qRT-PCR quantification (mean ± SEM) of the expression (IP/input) of five bacTRAP-enriched genes in bacTRAP (white bars) and three vTRAP serotype (gray bars) samples. Cbln1, Cbln4, Cldn1, and Nnat, $p < 0.05$ for IP versus input for all groups. ** $p < 0.01$; *** $p < 0.001$; **** $p < 0.0001$.

The scale bars represent 1 mm, except injection site insets in (C) (500 μ m). See also Figure S6 and Table S4.

species. Such an application of the technique may be used for understanding neuroplasticity, axonopathy, regeneration, and neurodegeneration.

The extremely high correlation between vTRAP and bacTRAP allows for the targeting and profiling of a single genetically determined cell population by either viral or transgenic approaches. This is particularly useful for cases where anatomical distinction is more easily achieved with viral injection rather than physical dissection. For example, vTRAP can be used with the *Slc17a6* (*Vglut2*) Cre-driver mice, in which all projection neurons in thalamus express Cre, to examine discrete thalamic nuclei or with dopamine receptor mice to target dorsal or ventral striatal structures. The localized nature of viral injections also enables the exploration of regional differences in gene expression in genetically similar cells within a single neural structure. This was exemplified in the *Ntsr1* cells by the discovery that vTRAP failed to enrich for genes expressed in cortical areas distal to the virus injection, establishing a high level of sensitivity in the approach and its potential to define molecularly distinct subdivisions of anatomical structures. Whereas methods for sequencing the transcriptomes of single cells have greatly improved in recent years, the higher sensitivity of vTRAP for detecting low-expressed cell-type-specific genes provides an advantage for unearthing subtle molecular differences that may result from experimental manipulation, such as behavior or pharmacological treatments.

Different AAV serotypes are known to have tropism for distinct cell types throughout the brain and body. The success of vTRAP experiments using viruses coated with three different capsid proteins implies that vTRAP is not limited by AAV serotype, making this technique amenable to characterizing a wide variety of cell types. However, we found that the AAV2 virus had limited spread in cortex and a number of the layer 6 marker genes were not as highly enriched in the AAV2 dataset when compared to the other serotypes and bacTRAP. This emphasizes the need to carefully test and select AAV serotypes that are most appropriate to target the cell type of interest, especially in less well-characterized brain regions or other tissues throughout the body.

AAVs have become indispensable tools that allow neuroscientists to functionally dissect disparate components of neural circuits *in vivo*. Vectors that deliver light-activated channels and pumps (channelrhodopsins, halorhodopsins, and archaerhodopsins), designer receptors (DREADDs), genetically encoded calcium indicators (GECIs), and small interfering RNAs (siRNAs) are widely available from academic and commercial sources. In addition, genome editing technologies, such as CRISPR, have advanced to the point where it is possible to acutely manipulate gene expression and epigenetic states using viral-mediated gene transfer (Ran et al., 2015). Multiplexing the vTRAP vectors we report here in tandem with the above approaches offers a comprehensive strategy to interrogate the precise role of individual, cell-type-specific genes in circuit function. These studies could facilitate our understanding of cell-type-specific molecular adaptations underlying changes in neural activity, the impact of targeted genetic alterations on cell function, as well as correlated behavioral alterations observed after such experimental perturbations. Such intersec-

tional strategies will enable the study of neural circuitry at a resolution not previously possible.

This study reports a rapid, spatially restricted tool for translational profiling of cell types that can be applied easily throughout the body. Previous approaches to molecular profiling within complex tissues were restricted to transgenic strategies that took significant amounts of time to generate new and/or cross multiple mouse strains and could potentially result in contamination from off-target cell populations from ontogenetic expression. The vTRAP technology now enables a rapid and highly anatomically restricted methodology, which can elucidate marker genes for specific subregions within a given tissue. The utility of the vTRAP approach for translational profiling arises from its rapidity, ease of use, and broad applicability to systems already utilizing adeno-associated viruses.

EXPERIMENTAL PROCEDURES

Animals

All procedures involving animals were approved by The Rockefeller University Institutional Animal Care and Use Committee and were in accordance with NIH guidelines. *Ntsr1*-bacTRAP (TS16), *Pmch*-Cre, and DAT-Cre mice were generated and maintained at The Rockefeller University and described previously (Doyle et al., 2008; Ekstrand et al., 2014; Jego et al., 2013; Knight et al., 2012). *Ntsr1*-Cre (GN220) and SERT-Cre (ET33) mice were generated by the GENSAT Project (Gong et al., 2007) and were purchased from the Mutant Mouse Regional Resource Center (Stock IDs 017266-UCD and 031028-UCD, respectively). The generation of *Abcb1a*-bacTRAP mice used for the specificity index is described in [Supplemental Experimental Procedures](#). All mice were bred on a C57BL/6J background and maintained on a 12-hr light-dark cycle. Animals used in the study were male and female. Mice were sacrificed at 10–20 weeks of age within the same circadian period (12:00–16:00).

Generation of AAVs

The plasmid pAAV-FLEX-EGFPL10a was generated by subcloning the EGFPL10a transgene into pAAV-EF1a-DIO-hChR2(H134R)-mCherry-WPRE-HGHPA (Addgene plasmid no. 20297) in the reverse orientation, replacing ChR2-mCherry. Plasmids were then packaged into AAVs at the University of North Carolina Vector Core or the University of Pennsylvania Vector Core. Virus titers were 1.63×10^{13} gc/mL for AAV5, 4.7×10^{12} gc/mL for AAV2, and 7.47×10^{12} gc/mL for AAV9. See [Supplemental Experimental Procedures](#) for more details.

Stereotaxic Surgeries

Bilateral stereotaxic injections of AAV-FLEX-EGFPL10a into adult (8–20 weeks old) Cre mice (male and female) under ketamine/xylazine (100/10 mg/kg) anesthesia were performed as described in [Supplemental Experimental Procedures](#). Animals were sacrificed 1–4 weeks after surgery, and tissue was collected for polysome IPs, histology, or polysome fractionation as described below.

Immunohistochemistry

Immunofluorescent staining was carried out on free-floating brain sections or adherent HEK293T cells and imaged on either a Zeiss LSM780 or LSM700 confocal microscope. For details, see [Supplemental Experimental Procedures](#).

TRAP

Affinity purification of EGFP-tagged polysomes was done 3 or 4 weeks after virus injections. Three biological replicates consisting of tissue pooled from three to five mice (mixed sex) were collected for each condition. IPs and RNA extractions were carried out as previously described (Heiman et al., 2014) and in [Supplemental Experimental Procedures](#). Briefly, brain tissue was homogenized in buffer containing 10 mM HEPES-KOH (pH 7.4),

150 mM KCl, 5 mM MgCl₂, 0.5 mM DTT, 100 µg/mL cycloheximide, RNasin (Promega) and SUPERase-In™ (Life Technologies) RNase inhibitors, and Complete-EDTA-free protease inhibitors (Roche) and then cleared by two-step centrifugation to isolate polysome-containing cytoplasmic supernatant. Polysomes were immunoprecipitated using monoclonal anti-EGFP antibodies (clones 19C8 and 19F7; see Heiman et al., 2008) bound to biotinylated-Protein L (Pierce; Thermo Fisher Scientific)-coated streptavidin-conjugated magnetic beads (Life Technologies), and bound RNA was purified using the Absolutely RNA Nanoprep kit (Agilent Technologies). RNA quantity was measured with a Nanodrop 1000 spectrophotometer, and quality was assayed on an Agilent 2100 Bioanalyzer. Only samples with RNA integrity values ≥ 7.0 were used for RNA-seq and qRT-PCR analyses.

RNA-Seq and qRT-PCR

For cortical samples, TRAP RNA was amplified using the Ovation RNA-Seq System V2 Kit (NuGEN), and RNA-seq libraries were prepared using the TruSeq RNA Sample Preparation Kit v2 (Illumina) following manufacturer's protocols. MCH neuron RNA-seq libraries were prepared using the SMARTer Ultra Low RNA Kit (Clontech Laboratories). Sequencing reactions were done using the Illumina HiSeq 2500 platform with three samples multiplexed per sequencing lane. RNA-seq reads were then aligned to annotated exons using the mm10 mouse reference genome with STAR (Dobin et al., 2013) version 2.0.0e_r291, and quantification of aligned reads was done using HTSeq (Anders et al., 2015) version 0.6.0. Differential expression was calculated by DESeq2 (Love et al., 2014) version 1.4.5, filtering for a false discovery rate (FDR) cutoff of <0.05 and $|\log_2|$ fold change >1.0 . Specificity index analysis was performed using the pSI (specificity index statistic) R-package version 1.1 (Dougherty et al., 2010; Xu et al., 2014). Detailed methods can be found in *Supplemental Experimental Procedures*.

The Taqman method was used for qRT-PCR analysis on three biological replicates for each condition using either an Applied Biosystems 7500 Fast or StepOnePlus Fast Real-Time PCR System. Data were normalized to *Rpl23* (Figures 2C, 3B, and S2) by standard curve or to *Actb* (Figures 4D and 6G) by the comparative C_T ($2^{-\Delta\Delta CT}$) method (Livak and Schmittgen, 2001).

Polysome Fractionation

Polysome fractionations were collected by centrifugation in a sucrose gradient as described previously (Darnell et al., 2011) and in *Supplemental Experimental Procedures*. Briefly, TCA-precipitated proteins from each fraction were analyzed by western blot, detected by enhanced chemiluminescence (Western Lightning Plus detection kit; PerkinElmer), and quantified by densitometry following film scans (Kodak MR film; ImageJ software).

Statistics

All data analysis was performed in Graphpad Prism, Microsoft Excel, or R (R Core Team, 2013). Student's t test was used to compare differences in qRT-PCR results between IP and input samples in Figures 2D, 3F, 4D, and 6G. Two-way ANOVA on the log₂ fold-change values was used to compare each of the vTRAP groups against bacTRAP for the specified genes in Figures 4D and 6G.

ACCESSION NUMBERS

The accession number for the raw RNA-seq datasets reported in this paper is GEO: GSE89737.

SUPPLEMENTAL INFORMATION

Supplemental Information includes Supplemental Experimental Procedures, six figures, and four tables and can be found with this article online at <http://dx.doi.org/10.1016/j.celrep.2017.03.048>.

AUTHOR CONTRIBUTIONS

A.R.N. and E.F.S. designed all experiments, and A.R.N., E.F.S., M.V.M., K.L.M., C.E.S., and M.I.E. performed all experiments. G.S.R. and K.S. per-

formed and analyzed polysome fractionations. B.C.F. assisted with IHC. A.R.N., E.F.S., M.V.M., M.I.E., Y.L., A.M., J.M.F., and N.H. analyzed data. A.R.N., N.H., and E.F.S. wrote the paper.

ACKNOWLEDGMENTS

This work was supported by the Howard Hughes Medical Institute (to J.M.F. and N.H.), the JPB Foundation (to J.M.F.), NIH/NIDA P30 Center DA035756 (to N.H.), NIH/NIMH Conte Center PHS MH090963 (to N.H.), Brain & Behavior Research Foundation NARSAD Young Investigator grant 21464 (to E.F.S.), the van Ameringen Foundation (to E.F.S.), Whitehall Foundation grant 2014-12-104 (to E.F.S.), NIH/NINDS R01NS091722 (to E.F.S.), and NSF INSPIRE Award 1343174 (to N.H. and E.F.S.). A.R.N. acknowledges support from The Rockefeller University, provided by the David Rockefeller Fellowship. We wish to thank The Rockefeller University Genomics and Bio-Imaging Resource Centers. We also thank Karl Deisseroth for contributing the plasmid pAAV-EF1a-DIO-ChR2-mCherry, Jennifer Darnell for assistance with polysome profiling, Marian Mellen and Juncheng Li for sharing the *Dlx1* bacTRAP sequencing data, and Eva B. Holzner for technical assistance.

Received: July 25, 2016

Revised: February 11, 2017

Accepted: March 14, 2017

Published: April 18, 2017

REFERENCES

- Anders, S., Pyl, P.T., and Huber, W. (2015). HTSeq—a Python framework to work with high-throughput sequencing data. *Bioinformatics* 31, 166–169.
- Aschauer, D.F., Kreuz, S., and Rumpel, S. (2013). Analysis of transduction efficiency, tropism and axonal transport of AAV serotypes 1, 2, 5, 6, 8 and 9 in the mouse brain. *PLoS ONE* 8, e76310.
- Atasoy, D., Aponte, Y., Su, H.H., and Sternson, S.M. (2008). A FLEX switch targets Channelrhodopsin-2 to multiple cell types for imaging and long-range circuit mapping. *J. Neurosci.* 28, 7025–7030.
- Crozier, S., Franchi-Bernard, G., Colard, C., Poncet, F., La Roche, A., and Risold, P.Y. (2010). A comparative analysis shows morphofunctional differences between the rat and mouse melanin-concentrating hormone systems. *PLoS ONE* 5, e15471.
- Darnell, J.C., Van Driesche, S.J., Zhang, C., Hung, K.Y., Mele, A., Fraser, C.E., Stone, E.F., Chen, C., Fak, J.J., Chi, S.W., et al. (2011). FMRP stalls ribosomal translocation on mRNAs linked to synaptic function and autism. *Cell* 146, 247–261.
- Dobin, A., Davis, C.A., Schlesinger, F., Drenkow, J., Zaleski, C., Jha, S., Batut, P., Chaisson, M., and Gingeras, T.R. (2013). STAR: ultrafast universal RNA-seq aligner. *Bioinformatics* 29, 15–21.
- Domingos, A.I., Sordillo, A., Dietrich, M.O., Liu, Z.W., Tellez, L.A., Vaynshteyn, J., Ferreira, J.G., Ekstrand, M.I., Horvath, T.L., de Araujo, I.E., and Friedman, J.M. (2013). Hypothalamic melanin concentrating hormone neurons communicate the nutrient value of sugar. *eLife* 2, e01462.
- Dougherty, J.D., Schmidt, E.F., Nakajima, M., and Heintz, N. (2010). Analytical approaches to RNA profiling data for the identification of genes enriched in specific cells. *Nucleic Acids Res.* 38, 4218–4230.
- Dougherty, J.D., Maloney, S.E., Wozniak, D.F., Rieger, M.A., Sonnenblick, L., Coppola, G., Mahieu, N.G., Zhang, J., Cai, J., Patti, G.J., et al. (2013). The disruption of *Celf6*, a gene identified by translational profiling of serotonergic neurons, results in autism-related behaviors. *J. Neurosci.* 33, 2732–2753.
- Doyle, J.P., Dougherty, J.D., Heiman, M., Schmidt, E.F., Stevens, T.R., Ma, G., Bupp, S., Shrestha, P., Shah, R.D., Doughty, M.L., et al. (2008). Application of a translational profiling approach for the comparative analysis of CNS cell types. *Cell* 135, 749–762.
- Drane, L., Ainsley, J.A., Mayford, M.R., and Reijmers, L.G. (2014). A transgenic mouse line for collecting ribosome-bound mRNA using the tetracycline trans-activator system. *Front. Mol. Neurosci.* 7, 82.

- Ekstrand, M.I., Nectow, A.R., Knight, Z.A., Latcha, K.N., Pomeranz, L.E., and Friedman, J.M. (2014). Molecular profiling of neurons based on connectivity. *Cell* **157**, 1230–1242.
- Franklin, K.B.J., and Paxinos, G. (2008). *The Mouse Brain in Stereotaxic Coordinates*, Third Edition (Amsterdam, Boston: Elsevier Academic Press).
- Galazo, M.J., Emsley, J.G., and Macklis, J.D. (2016). Corticothalamic projection neuron development beyond subtype specification: Fog2 and intersectional controls regulate intraclass neuronal diversity. *Neuron* **91**, 90–106.
- Gerfen, C.R., Paletzki, R., and Heintz, N. (2013). GENSAT BAC cre-recombinase driver lines to study the functional organization of cerebral cortical and basal ganglia circuits. *Neuron* **80**, 1368–1383.
- Gong, S., Doughty, M., Harbaugh, C.R., Cummins, A., Hatten, M.E., Heintz, N., and Gerfen, C.R. (2007). Targeting Cre recombinase to specific neuron populations with bacterial artificial chromosome constructs. *J. Neurosci.* **27**, 9817–9823.
- Gorski, J.A., Talley, T., Qiu, M., Puelles, L., Rubenstein, J.L., and Jones, K.R. (2002). Cortical excitatory neurons and glia, but not GABAergic neurons, are produced in the Emx1-expressing lineage. *J. Neurosci.* **22**, 6309–6314.
- Grgic, I., Krautberger, A.M., Hofmeister, A., Lalli, M., DiRocco, D.P., Fleig, S.V., Liu, J., Duffield, J.S., McMahon, A.P., Aronow, B., and Humphreys, B.D. (2014). Translational profiles of medullary myofibroblasts during kidney fibrosis. *J. Am. Soc. Nephrol.* **25**, 1979–1990.
- Heiman, M., Schaefer, A., Gong, S., Peterson, J.D., Day, M., Ramsey, K.E., Suárez-Fariñas, M., Schwarz, C., Stephan, D.A., Surmeier, D.J., et al. (2008). A translational profiling approach for the molecular characterization of CNS cell types. *Cell* **135**, 738–748.
- Heiman, M., Kulicke, R., Fenster, R.J., Greengard, P., and Heintz, N. (2014). Cell type-specific mRNA purification by translating ribosome affinity purification (TRAP). *Nat. Protoc.* **9**, 1282–1291.
- Jego, S., Glasgow, S.D., Herrera, C.G., Ekstrand, M., Reed, S.J., Boyce, R., Friedman, J., Burdakov, D., and Adamantidis, A.R. (2013). Optogenetic identification of a rapid eye movement sleep modulatory circuit in the hypothalamus. *Nat. Neurosci.* **16**, 1637–1643.
- Kaspar, B.K., Vissel, B., Bengoechea, T., Crone, S., Randolph-Moore, L., Muller, R., Brandon, E.P., Schaffer, D., Verma, I.M., Lee, K.F., et al. (2002). Adeno-associated virus effectively mediates conditional gene modification in the brain. *Proc. Natl. Acad. Sci. USA* **99**, 2320–2325.
- Knight, Z.A., Tan, K., Birsoy, K., Schmidt, S., Garrison, J.L., Wysocki, R.W., Emiliano, A., Ekstrand, M.I., and Friedman, J.M. (2012). Molecular profiling of activated neurons by phosphorylated ribosome capture. *Cell* **151**, 1126–1137.
- Lake, B.B., Ai, R., Kaeser, G.E., Salathia, N.S., Yung, Y.C., Liu, R., Wildberg, A., Gao, D., Fung, H.L., Chen, S., et al. (2016). Neuronal subtypes and diversity revealed by single-nucleus RNA sequencing of the human brain. *Science* **352**, 1586–1590.
- Lam, D.D., Leininger, G.M., Louis, G.W., Garfield, A.S., Marston, O.J., Leshan, R.L., Scheller, E.L., Christensen, L., Donato, J., Jr., Xia, J., et al. (2011). Leptin does not directly affect CNS serotonin neurons to influence appetite. *Cell Metab.* **13**, 584–591.
- Lein, E.S., Hawrylycz, M.J., Ao, N., Ayres, M., Bensinger, A., Bernard, A., Boe, A.F., Boguski, M.S., Brockway, K.S., Byrnes, E.J., et al. (2007). Genome-wide atlas of gene expression in the adult mouse brain. *Nature* **445**, 168–176.
- Liu, J., Krautberger, A.M., Sui, S.H., Hofmann, O.M., Chen, Y., Baetscher, M., Grgic, I., Kumar, S., Humphreys, B.D., Hide, W.A., and McMahon, A.P. (2014). Cell-specific translational profiling in acute kidney injury. *J. Clin. Invest.* **124**, 1242–1254.
- Livak, K.J., and Schmittgen, T.D. (2001). Analysis of relative gene expression data using real-time quantitative PCR and the 2(-Delta Delta C(T)) method. *Methods* **25**, 402–408.
- Love, M.I., Huber, W., and Anders, S. (2014). Moderated estimation of fold change and dispersion for RNA-seq data with DESeq2. *Genome Biol.* **15**, 550.
- Madisen, L., Zwingman, T.A., Sunkin, S.M., Oh, S.W., Zariwala, H.A., Gu, H., Ng, L.L., Palmiter, R.D., Hawrylycz, M.J., Jones, A.R., et al. (2010). A robust and high-throughput Cre reporting and characterization system for the whole mouse brain. *Nat. Neurosci.* **13**, 133–140.
- Mellén, M., Ayata, P., Dewell, S., Kriaucionis, S., and Heintz, N. (2012). MeCP2 binds to 5hmC enriched within active genes and accessible chromatin in the nervous system. *Cell* **151**, 1417–1430.
- Nakajima, M., Görlich, A., and Heintz, N. (2014). Oxytocin modulates female sociosexual behavior through a specific class of prefrontal cortical interneurons. *Cell* **159**, 295–305.
- Nectow, A.R., Ekstrand, M.I., and Friedman, J.M. (2015). Molecular characterization of neuronal cell types based on patterns of projection with Retro-TRAP. *Nat. Protoc.* **10**, 1319–1327.
- Oguchi, M., Okajima, M., Tanaka, S., Koizumi, M., Kikusui, T., Ichihara, N., Kato, S., Kobayashi, K., and Sakagami, M. (2015). Double virus vector infection to the prefrontal network of the macaque brain. *PLoS ONE* **10**, e0132825.
- Padilla, S.L., Carmody, J.S., and Zeltser, L.M. (2010). Pomp-expressing progenitors give rise to antagonistic neuronal populations in hypothalamic feeding circuits. *Nat. Med.* **16**, 403–405.
- Price, J.C., Guan, S., Burlingame, A., Prusiner, S.B., and Ghaemmaghami, S. (2010). Analysis of proteome dynamics in the mouse brain. *Proc. Natl. Acad. Sci. USA* **107**, 14508–14513.
- R Core Team (2013). *R: A Language and Environment for Statistical Computing* (Vienna, Austria: R Foundation for Statistical Computing).
- Ran, F.A., Cong, L., Yan, W.X., Scott, D.A., Gootenberg, J.S., Kriz, A.J., Zetsche, B., Shalem, O., Wu, X., Makarova, K.S., et al. (2015). In vivo genome editing using Staphylococcus aureus Cas9. *Nature* **520**, 186–191.
- Sanz, E., Yang, L., Su, T., Morris, D.R., McKnight, G.S., and Amieux, P.S. (2009). Cell-type-specific isolation of ribosome-associated mRNA from complex tissues. *Proc. Natl. Acad. Sci. USA* **106**, 13939–13944.
- Schmidt, E.F., Warner-Schmidt, J.L., Otopalik, B.G., Pickett, S.B., Greengard, P., and Heintz, N. (2012). Identification of the cortical neurons that mediate antidepressant responses. *Cell* **149**, 1152–1163.
- Schwarz, L.A., Miyamichi, K., Gao, X.J., Beier, K.T., Weissbourd, B., DeLoach, K.E., Ren, J., Ibanes, S., Malenka, R.C., Kremer, E.J., and Luo, L. (2015). Viral-genetic tracing of the input-output organization of a central noradrenaline circuit. *Nature* **524**, 88–92.
- Shigeoka, T., Jung, H., Jung, J., Turner-Bridger, B., Ohk, J., Lin, J.Q., Amieux, P.S., and Holt, C.E. (2016). Dynamic axonal translation in developing and mature visual circuits. *Cell* **166**, 181–192.
- Shimada, M., Tritos, N.A., Lowell, B.B., Flier, J.S., and Maratos-Flier, E. (1998). Mice lacking melanin-concentrating hormone are hypophagic and lean. *Nature* **396**, 670–674.
- Shrestha, P., Mousa, A., and Heintz, N. (2015). Layer 2/3 pyramidal cells in the medial prefrontal cortex moderate stress induced depressive behaviors. *eLife* **4**, e08752.
- Sorensen, S.A., Bernard, A., Menon, V., Royall, J.J., Glattfelder, K.J., Desta, T., Hirokawa, K., Mortrud, M., Miller, J.A., Zeng, H., et al. (2015). Correlated gene expression and target specificity demonstrate excitatory projection neuron diversity. *Cereb. Cortex* **25**, 433–449.
- Stanley, S., Domingos, A.I., Kelly, L., Garfield, A., Damanpour, S., Heisler, L., and Friedman, J. (2013). Profiling of glucose-sensing neurons reveals that GHRH neurons are activated by hypoglycemia. *Cell Metab.* **18**, 596–607.
- Taniguchi, H., He, M., Wu, P., Kim, S., Paik, R., Sugino, K., Kvitsiani, D., Fu, Y., Lu, J., Lin, Y., et al. (2011). A resource of Cre driver lines for genetic targeting of GABAergic neurons in cerebral cortex. *Neuron* **71**, 995–1013.
- Tasic, B., Menon, V., Nguyen, T.N., Kim, T.K., Jarsky, T., Yao, Z., Levi, B., Gray, L.T., Sorensen, S.A., Dolbeare, T., et al. (2016). Adult mouse cortical cell taxonomy revealed by single cell transcriptomics. *Nat. Neurosci.* **19**, 335–346.
- Witten, I.B., Steinberg, E.E., Lee, S.Y., Davidson, T.J., Zalociusky, K.A., Brodsky, M., Yizhar, O., Cho, S.L., Gong, S., Ramakrishnan, C., et al. (2011).

- Recombinase-driver rat lines: tools, techniques, and optogenetic application to dopamine-mediated reinforcement. *Neuron* 72, 721–733.
- Xu, X., Wells, A.B., O'Brien, D.R., Nehorai, A., and Dougherty, J.D. (2014). Cell type-specific expression analysis to identify putative cellular mechanisms for neurogenetic disorders. *J. Neurosci.* 34, 1420–1431.
- Yoon, B.C., Jung, H., Dwivedy, A., O'Hare, C.M., Zivraj, K.H., and Holt, C.E. (2012). Local translation of extranuclear lamin B promotes axon maintenance. *Cell* 148, 752–764.
- Zeisel, A., Muñoz-Manchado, A.B., Codeluppi, S., Lönnerberg, P., La Manno, G., Juréus, A., Marques, S., Munguba, H., He, L., Betsholtz, C., et al. (2015). Brain structure. Cell types in the mouse cortex and hippocampus revealed by single-cell RNA-seq. *Science* 347, 1138–1142.
- Zhang, Y., Chen, K., Sloan, S.A., Bennett, M.L., Scholze, A.R., O'Keefe, S., Phatnani, H.P., Guarneri, P., Caneda, C., Ruderisch, N., et al. (2014). An RNA-sequencing transcriptome and splicing database of glia, neurons, and vascular cells of the cerebral cortex. *J. Neurosci.* 34, 11929–11947.
- Zhou, P., Zhang, Y., Ma, Q., Gu, F., Day, D.S., He, A., Zhou, B., Li, J., Stevens, S.M., Romo, D., and Pu, W.T. (2013). Interrogating translational efficiency and lineage-specific transcriptomes using ribosome affinity purification. *Proc. Natl. Acad. Sci. USA* 110, 15395–15400.

Supplemental Information

**Rapid Molecular Profiling of Defined
Cell Types Using Viral TRAP**

Alexander R. Nectow, Maria V. Moya, Mats I. Ekstrand, Awni Mousa, Kelly L. McGuire, Caroline E. Sferrazza, Bianca C. Field, Gabrielle S. Rabinowitz, Kirsty Sawicka, Yupu Liang, Jeffrey M. Friedman, Nathaniel Heintz, and Eric F. Schmidt

SUPPLEMENTAL INFORMATION

Figure S1

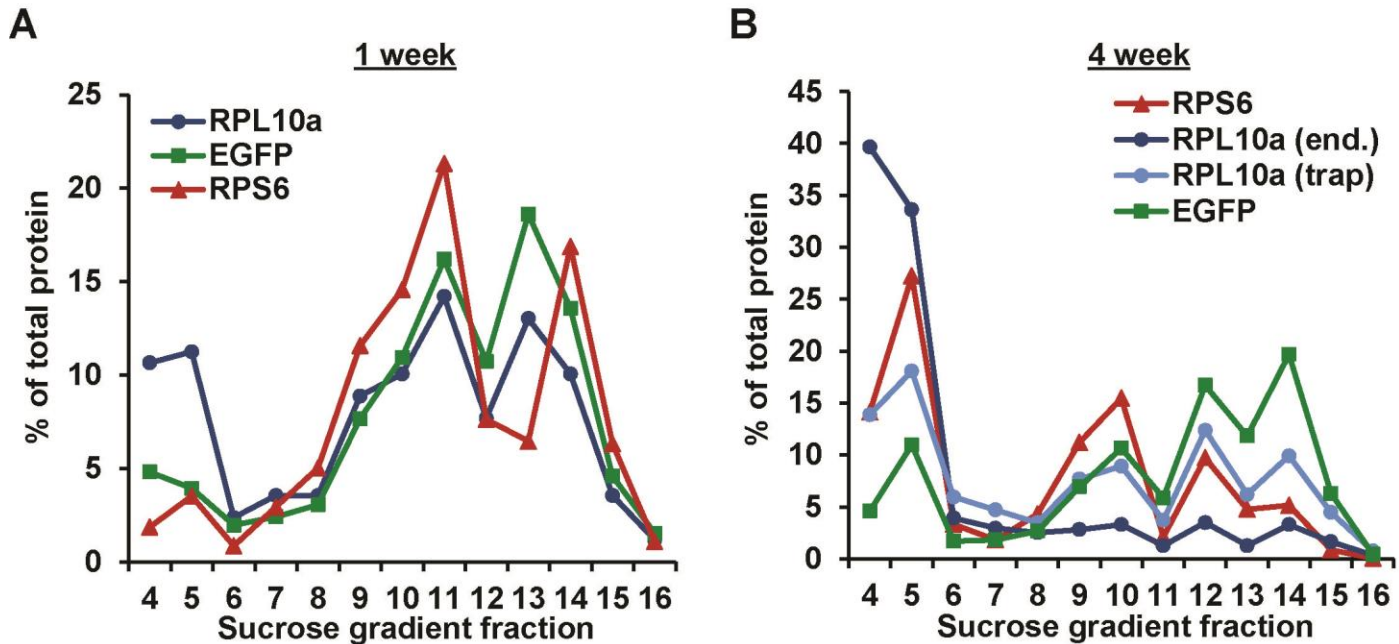


Figure S1. Quantification of the Distribution of Ribosomal Proteins in Polysome Fractions, Related to Figure 1.

(A) The distribution of RPS6, endogenous RPL10a, and EGFP-L10a was quantified for each sucrose gradient fraction after one week of AAV-FLEX-EGFP-L10a virus expression in Emx1-Cre cortex. The optical densities (OD) of each band on the Western blots from Figure 1E are shown as a percent of the sum of ODs across all fractions for each protein. The relative distribution of all three proteins overlapped across fractions.

(B) Quantification of the distribution of ribosomal proteins after four weeks of expression was calculated as in A. The distribution of both endogenous RPL10a (end.) and EGFP-L10a (trap) were quantified from the anti-RPL10a blot. While the relative pattern of distribution of each protein was consistent across each fraction, a significant amount of endogenous RPL10a was found in fractions 4 and 5 (corresponding to the 60S subunit and monosomes, respectively), leading to comparatively lower amounts of endogenous RPL10a in polysome fractions.

Figure S2

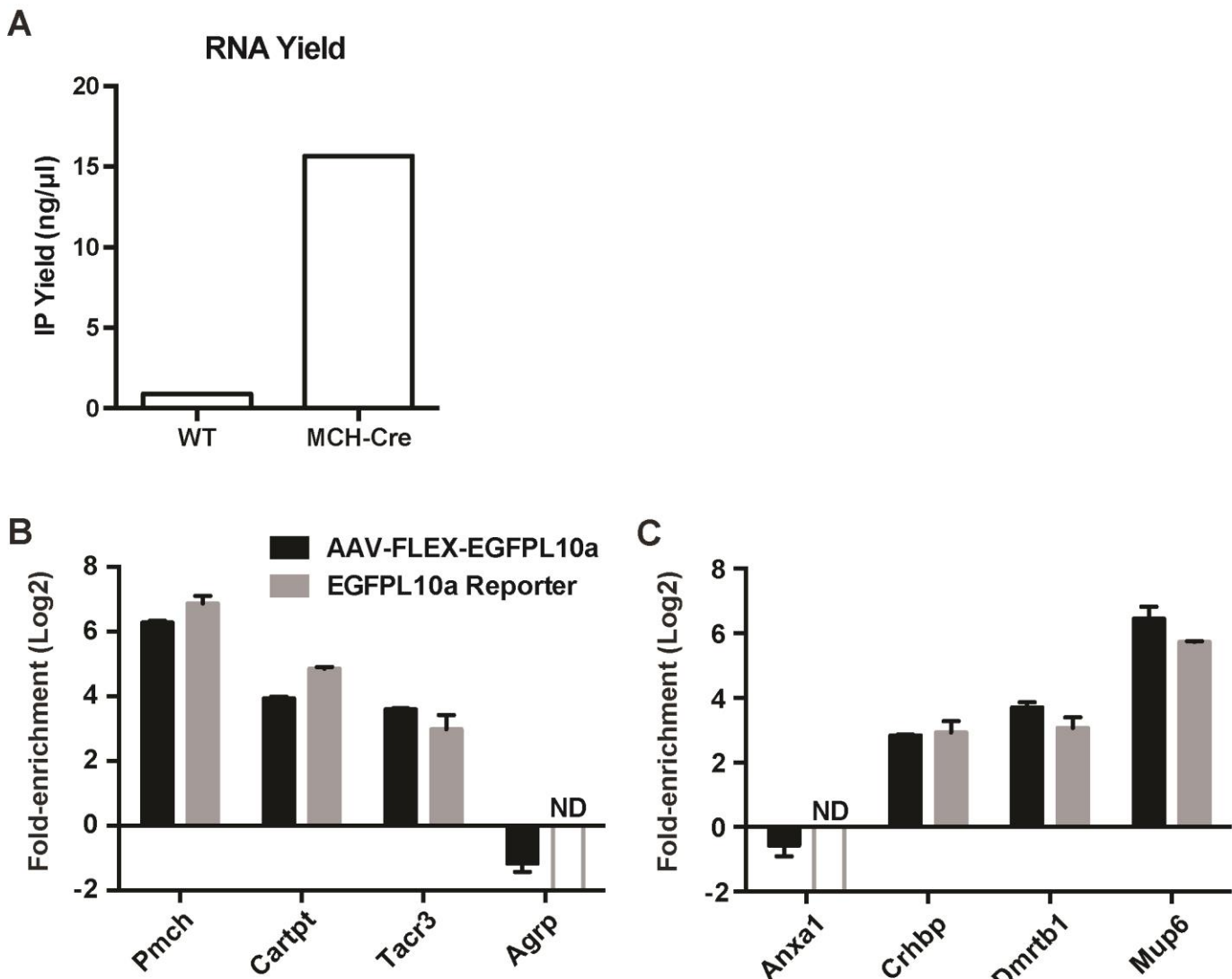


Figure S2. Comparative Enrichments from MCH Neurons using vTRAP and an EGFPL10a Reporter Mouse, Related to Figure 3.

(A) Total RNA yields after TRAP IPs in *Pmch*-Cre (MCH-Cre) mice or wildtype littermates (WT) following AAV-FLEX-EGFPL10a injections into the lateral hypothalamus.

(B) Quantitative RT-PCR comparison (Mean \pm SEM) of MCH neuron marker genes (*Pmch*, *Cartpt*, *Tacr3*) and a non-MCH, hypothalamic (arcuate) marker gene (*Agrp*) after IPs from the hypothalamus of *Pmch*-Cre mice using vTRAP (black bars) or crossed to the Rosa26^{fSTRAP} reporter (gray bars).

(C) Quantitative RT-PCR comparison (Mean \pm SEM) of a non-MCH neuron, midbrain marker gene (*Anxa1*), and newly-identified MCH neuron marker genes (*Crhbp*, *Dmrtb1*, *Mup6*) after IPs from the hypothalamus using vTRAP (black bars) or Rosa26^{fSTRAP} reporter (gray bars).

All data are displayed as mean \pm SEM. ND, the IP RNA was not detected.

Figure S3

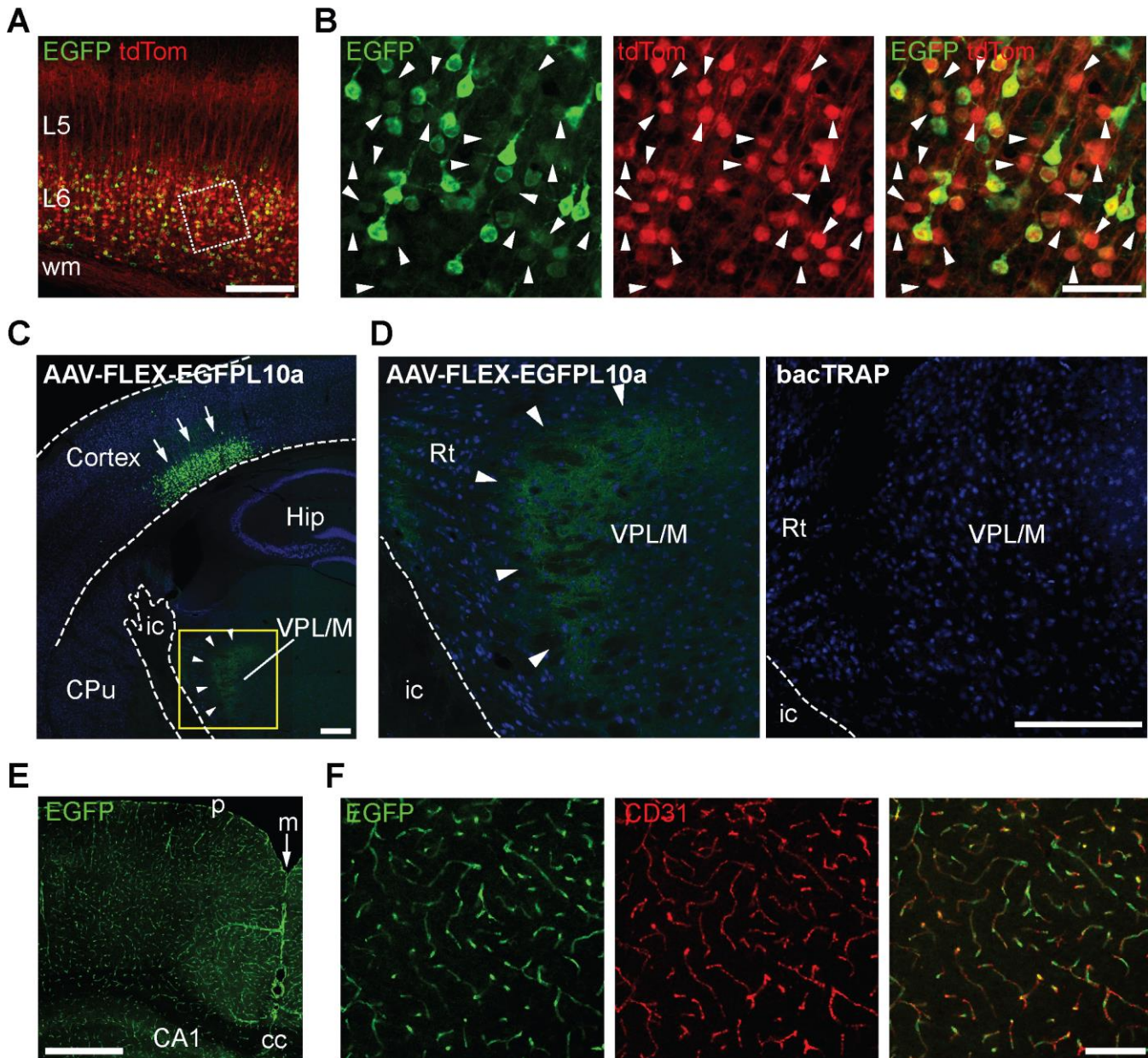


Figure S3. Co-labeling of L6 Cells by Ntsr1-bacTRAP and Ntsr1-Cre, and EGFP/EGFPL10a Expression in Abcb1a-bacTRAP Mice, Related to Figures 4 and 5.

(A) Low magnification image of EGFP (green) and tdTomato (tdTom; red) immunofluorescence in cortex from a Ntsr1-bacTRAP::Ntsr1-Cre::Rosa26^{tdTomato} mouse showing all labeled cells restricted to layer 6. L5, cortical layer 5; L6, cortical layer 6; wm, white matter. Scale bar, 200 μm.

(B) Higher magnification of boxed area in A showing co-labeling of EGFP and tdTomato in L6 cells. The expression levels of EGFP varied throughout the population, likely due to the activity of the BAC promoter, nearly all tdTomato+ cells were EGFP+ and vice versa. Arrowheads indicate double-labeled cells with very low EGFP expression. Scale bar, 50 μm.

(C) Low magnification image of EGFP (green) and NeuN (blue) immunofluorescence from a brain of a Ntsr1-Cre mouse that received an injection of AAV-FLEX-EGFPL10a into somatosensory cortex. EGFP expression can be seen in the cell bodies in the cortex (arrows) as well as the axon terminal fields in the thalamus (arrowheads). Image was taken from a composite of a tiled scan of a coronal brain slice. CPu, caudate-putamen; Hip, hippocampus; ic, internal capsule; VPL/M, ventral posterolateral and ventral posteromedial nuclei of thalamus. Scale bar, 250 μm.

(D) Left panel shows a higher magnification of the boxed area in C and the right panel is the equivalent region from a Ntsr1-bacTRAP mouse. Note the visible EGFP expression in the axon terminal fields of a Cre mouse injected with the AAV-FLEX-EGFPL10a virus

(arrowheads) but not in the bacTRAP mouse. ic, internal capsule; Rt, reticular thalamic nucleus; VPL/M, ventral posterolateral and ventral posteromedial nuclei of thalamus. Scale bar, 250 μ m.

(E) Low magnification image of anti-EGFP immunofluorescence in cortex from an *Abcb1a*-bacTRAP ES3026 mouse. CA1, CA1 field of hippocampal formation; cc, corpus callosum; m, midline; p, pial surface. Scale bar, 500 μ m.

(F) Higher magnification image of cortex of *Abcb1a*-bacTRAP mouse showing co-labeling of anti-EGFP (green) with anti-CD31, an endothelial cell marker (Pecam1, red). Scale bar, 100 μ m.

Figure S4

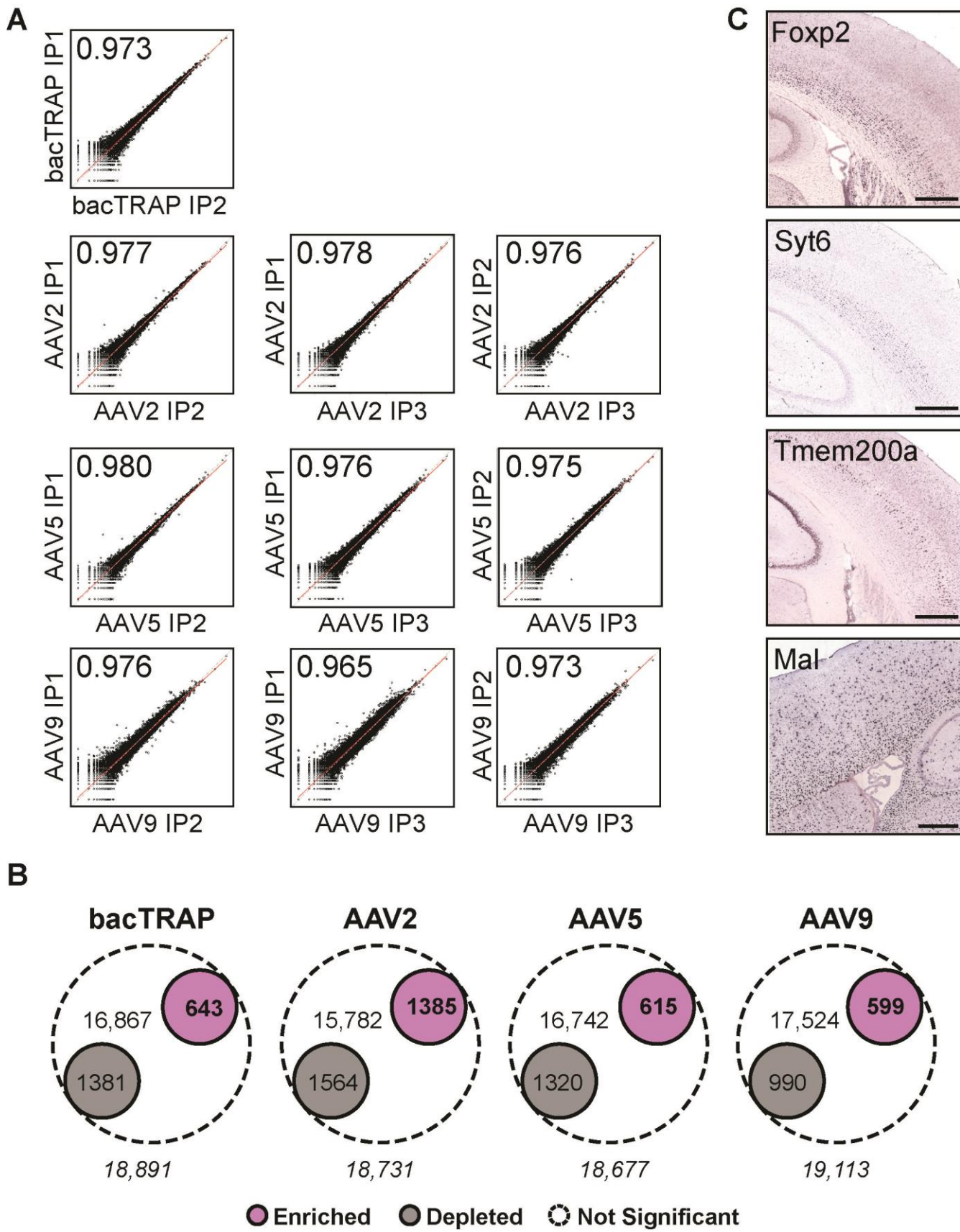


Figure S4. Correlation of bacTRAP and vTRAP Replicates and Quantification of Differentially Expressed Genes Between IP

and Input Samples, Related to Figure 4.

(A) Scatter plots comparing the normalized counts of all genes between individual replicate IPs from bacTRAP and vTRAP samples from AAV2, AAV5, and AAV9. The coefficient of determination (r^2) for each comparison is displayed in the top left corner.

(B) Venn diagrams indicating the number of genes significantly enriched in the TRAP IP (purple), the number of genes significantly depleted from the IPs (gray) and the number of genes not enriched or depleted in the bacTRAP and vTRAP experiments. Total number of genes with mapped reads in each experiment is in italics at the bottom.

(C) ABA ISH showing the cortex expression of neuronal genes *Foxp2* (layer 6, coronal), *Syt6* (layer 6, coronal), *Tmem200a* (layer 5, coronal), and the oligodendroglia marker, *Mal* (sagittal). Scale bars, 500 μ m.

Figure S5

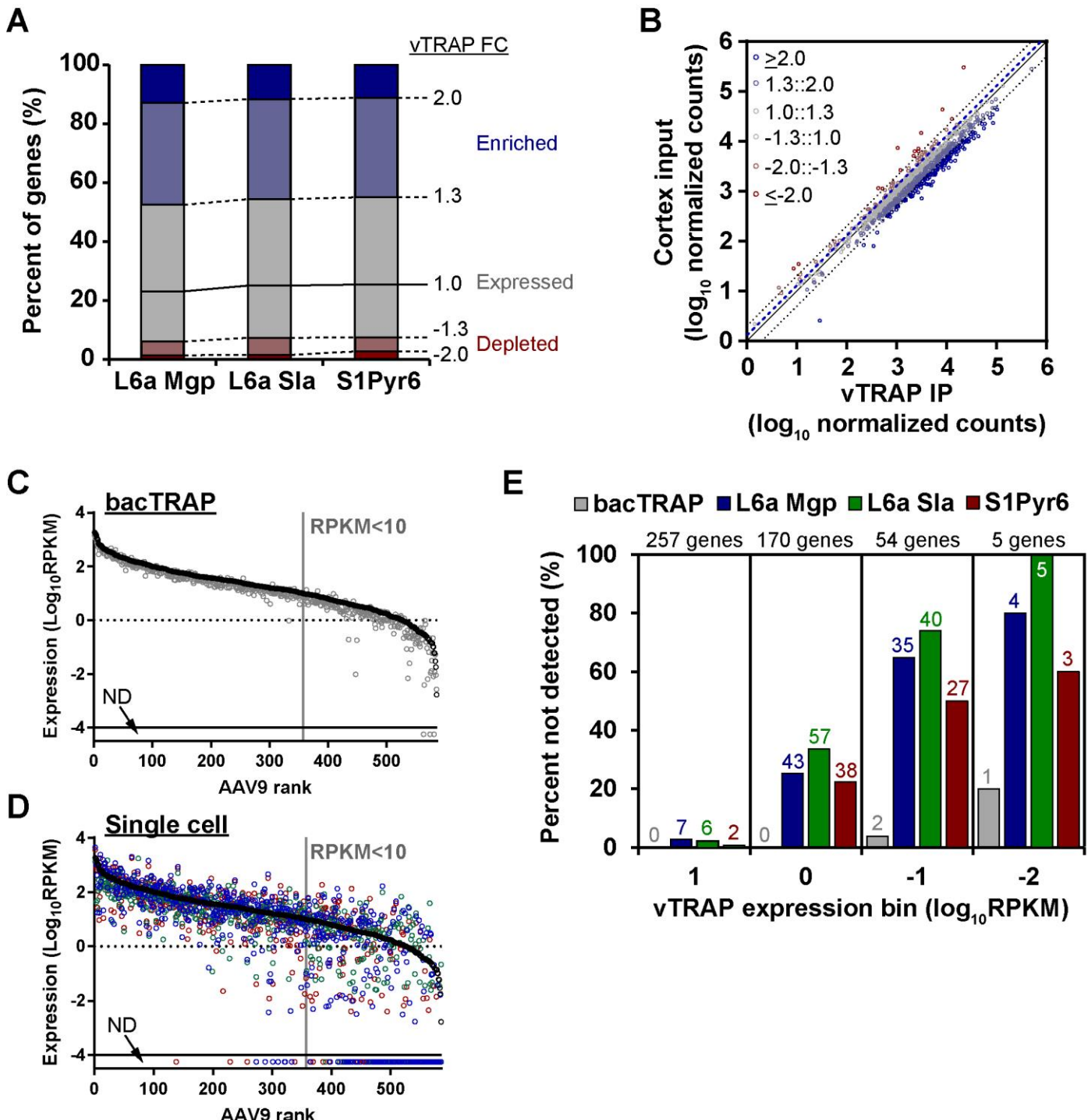


Figure S5. Comparison of vTRAP to Representative Single Cell RNA-seq Data Sets, Related to Figure 5.

(A) The top 1000 highest expressed genes were identified for three published single cell RNA-seq data sets comprised of layer 6 pyramidal cell populations: “L6a Mgp,” “L6a Sla,” (Tasic 2016) and “S1Pyr6” (Zeisel 2015). For each gene, the fold change was determined in the AAV9 vTRAP IP over input and the proportion of genes highly enriched (dark blue), enriched (light blue), expressed (not strongly enriched or depleted, gray), depleted (light red), or highly depleted (dark red) were plotted in a stacked bar graph. The fold change cutoff for each category is indicated on the right (vTRAP FC). More than 75% of the genes on each data set had a fold change >1.0 (over 92% of the genes from each data set were in the “expressed” range or higher) with over 45% being enriched greater than 1.3-fold in the IPs, demonstrating the sensitivity of vTRAP.

(B) Scatter plot of vTRAP IP (x-axis) and whole cortex input (y-axis) normalized counts for the top 1000 genes expressed in the L6a Mgp single cell data set. Genes are colored based on vTRAP fold change bins as in A. Dotted lines show 2-fold enrichment and

depletion and solid gray line indicates the origin. Dashed blue line shows -1.3-fold change, with “expressed” genes found to the right of the line.

(C) vTRAP enriched genes ($\log_2\text{FC}>1$) were ranked based on their expression ($\log_{10}\text{RPKM}$) from highest to lowest (left to right) expression values were plotted for vTRAP IPs (black circles) and bacTRAP IPs (gray circles). The bar at the bottom indicates genes where $\text{RPKM}=0$ (not detected, ND). The bacTRAP expression values correlate very highly with those of vTRAP, with only three low-expressed genes failing to be detected by bacTRAP.

(D) vTRAP enriched genes are plotted as in C with the expression values from three single cell data sets (L6a Mgp, blue; L6a Sla, green; S1Pyr6, red). The comparative expression for each gene was much more variable compared to bacTRAP (C), and many low-expressed genes in the vTRAP data were not detected in the single cell samples.

(E) Low expressed vTRAP genes were binned based on expression and the percent of genes in each bin with $\text{RPKM}=0$ in bacTRAP and single cell data sets was quantified. The total number of genes in each bin is indicated at the top and the number of genes not detected is written above each bar.

Figure S6

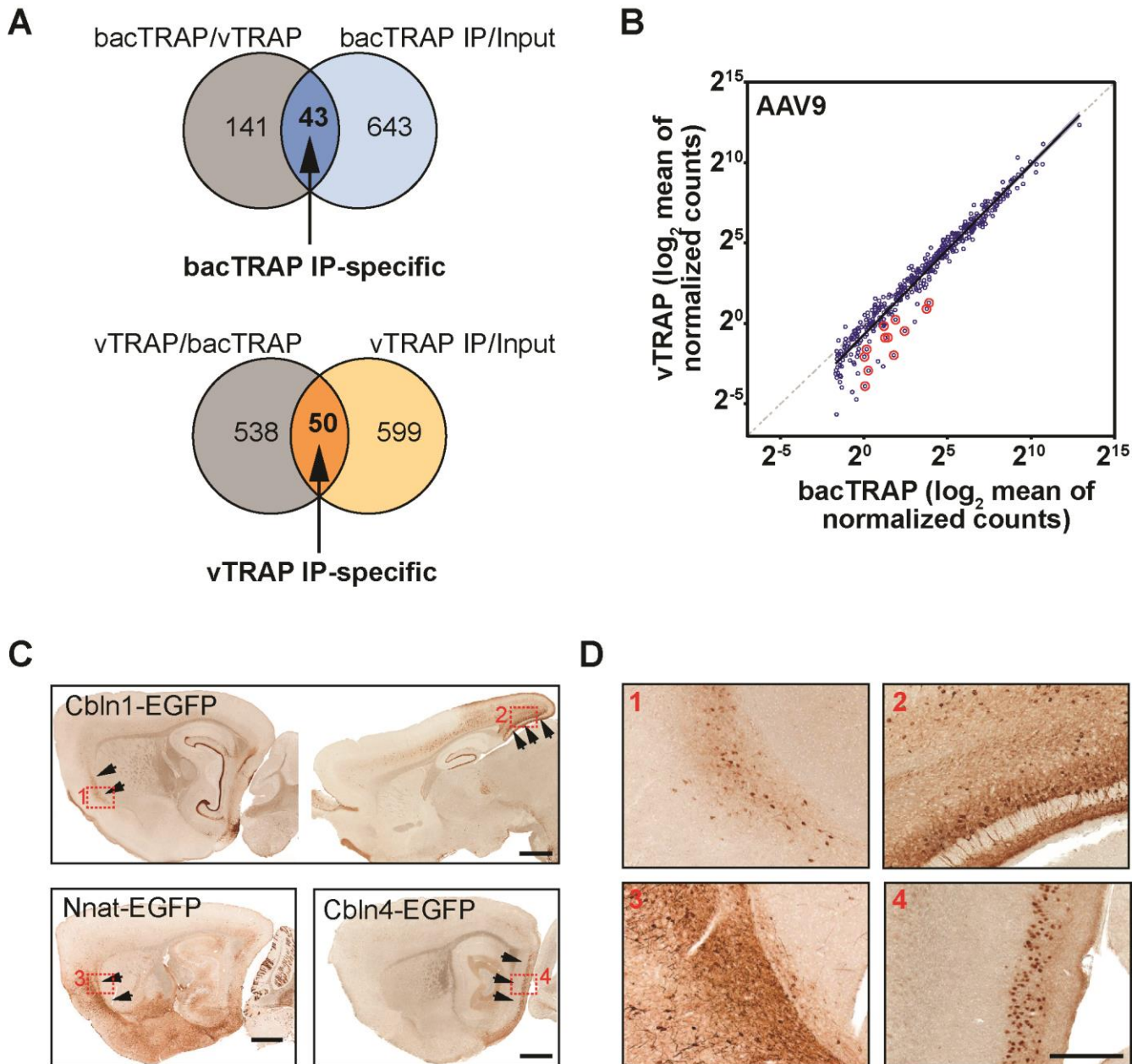


Figure S6. Identification of VTRAP-Specific and bacTRAP-Specific Genes, Related to Figure 6.

(A) Venn diagrams illustrating the definition of bacTRAP IP-specific genes as the union (blue) of genes significantly enriched in bacTRAP IP versus whole cortex input and bacTRAP IP versus vTRAP IP (top), and the definition of vTRAP IP-specific genes as the union (orange) of genes significantly enriched in vTRAP IP versus whole cortex input and vTRAP IP versus bacTRAP IP (bottom). vTRAP samples were from AAV9 injections. All significant genes had \log_2 fold change >1.0 and FDR <0.1 .

(B) Genes with regional expression (red circles) are indicated on the scatter plot from Figure 5C comparing the expression of CTthal specific genes ($pSI < 0.05$; blue circles) between Ntsr1 bacTRAP (x-axis) and AAV9 vTRAP (y-axis). Regional genes account for a majority of the CTthal specific genes that are considerably enriched in the bacTRAP samples.

(C) Anti-EGFP immunolabeling of BAC reporter lines showing expression patterns of some regionally expressed genes absent from vTRAP data set. Arrowheads identify regions with high expression in cells. Scale bars, 1 μ m.

(D) High magnification images from boxed areas in D. Scale bar, 200 μ m. Images in D and E are from The Gene Expression Nervous System Atlas (Gong et al., 2003) (www.gensat.org). Scale bars, 200 μ m.

Table S1. bacTRAP Transgenic Mouse Strains used for Specificity Index, Related to Figure 5.

Driver Gene	Founder	Cell type	Reference
Abcb1a	ES3026	Blood vessels	This paper
Aldh1l1	JD130	Astrocytes	Doyle et al. (2008)
Dlx1	GM520	Fast-spiking interneurons	Nakajima et al. (2014)
Glt25d2	DU9	Layer 5b CPn neurons	Doyle et al. (2008)
Ntsr1	TS16	Layer 6 CThal neurons	Doyle et al. (2008)
S100a10	ES691	Layer 5a CStr neurons; pia	Schmidt et al. (2012)

Table S2. Ntsr1-Specific Genes, Related to Figure 5.

The Specificity Index algorithm (Dougherty et al., 2010) was used to generate a list of genes specific for Ntsr1-expressing neurons compared to other cell types in the cortex (see Supplementary Table 1). The rank of each gene in each cell type and pSI is indicated. (Table is attached at the end of this document.)

Table S3. Previously identified cell type specific genes, Related to Figure 5.

This table contains a compiled list of genes that were previously shown to label L6 projection neurons or glial cells by a variety of distinct methodologies. The log₂ fold change (TRAP IP/input) of each gene is shown for each replicate of bacTRAP and vTRAP data sets. In addition, a summary of the methodology used, the cell type ID, and a hyperlink to the original source are also included. Genes appearing multiple times on the list are shown in bold. For glial genes, only the top 10 genes from each study are listed for each cell type. (Table is attached at the end of this document.)

Table S4. Images of Gene Expression Obtained from Public Databases, Related to Figures 6 and S3.**I. Allen Mouse Brain Atlas (mouse.brain-map.org)**

Figure	Symbol	Gene Name	Plane	Experiment	Image
6C	<i>Cbln1</i>	cerebellin 1 precursor protein	sagittal	100145395	61
6C	<i>Cbln1</i>	cerebellin 1 precursor protein	sagittal	100145395	109
6C	<i>Col23a1</i>	collagen, type XXIII, alpha 1	sagittal	71579924	110
6C	<i>Ly6g6e</i>	lymphocyte antigen 6 complex, locus G6E	sagittal	75198208	112
6C	<i>Nnat</i>	neuronatin	sagittal	77790710	41
6C	<i>Nnat</i>	neuronatin	sagittal	77790710	113
6D	<i>Ntsr1</i>	neurotensin receptor 1	sagittal	80342232	29
6E	<i>Cbln4</i>	cerebellin 4 precursor protein	sagittal	69540435	26
6E	<i>Cldn1</i>	claudin 1	sagittal	75695650	33
6E	<i>Fam70b</i>	family with sequence similarity 70, member B	sagittal	70298238	14
6E	<i>Lef1</i>	lymphoid enhancer binding factor 1	sagittal	77464846	28
6E	<i>Mum111</i>	melanoma associated antigen (mutated) 1-like 1	sagittal	71494629	42
6E	<i>Pth2r</i>	parathyroid hormone 2 receptor	sagittal	69863250	40
S3D	<i>Foxp2</i>	forkhead box P2	coronal	72079884	264
S3D	<i>Mal</i>	myelin and lymphocyte protein, T cell differentiation protein	sagittal	386243	101
S3D	<i>Syt6</i>	synaptotagmin VI	coronal	1032	215
S3D	<i>Tmem200a</i>	transmembrane protein 200A	coronal	79591403	262

II. GENSAT (www.gensat.org)

Figure	Symbol	Gene Name	Plane	Founder	Age	Section
S5D	<i>Cbln1</i>	cerebellin 1 precursor protein	sagittal	JD6	Adult	02
S5D	<i>Cbln1</i>	cerebellin 1 precursor protein	sagittal	JD6	Adult	08
S5D	<i>Nnat</i>	neuronatin	sagittal	EA106	Adult	03
S5D	<i>Cbln4</i>	cerebellin 4 precursor protein	sagittal	IG145	Adult	02

SUPPLEMENTAL EXPERIMENTAL PROCEDURES

Animals

All procedures involving animals were approved by The Rockefeller University Institutional Animal Care and Use Committee and were in accordance with National Institutes of Health guidelines. Ntsr1-bacTRAP (TS16), Pmch-Cre, and DAT-Cre mice were generated and maintained at The Rockefeller University and described previously (Doyle et al., 2008; Ekstrand et al., 2014; Jego et al., 2013; Knight et al., 2012). Ntsr1-Cre (GN220) and SERT-Cre (ET33) mice were generated by the GENSAT Project (Gong et al., 2007) and were purchased from the Mutant Mouse Regional Resource Center (Stock IDs 017266-UCD and 031028-UCD, respectively). Rosa26^{tdTomato} (Stock #007914) and Rosa26^{fsTRAP} (Stock #022367) mice were purchased from The Jackson Laboratories. All mice were bred on a C57BL/6J background and maintained on a 12 hr light-dark cycle. Animals used in the study were male and female. Mice were sacrificed at 10-20 weeks of age within the same circadian period (12:00-16:00).

To generate the Abcb1a-bacTRAP mice, the RP24-384G12 BAC, which contained the Abcb1a locus, was modified using the two-plasmid/one recombination protocol as described previously (Gong et al., 2010; Gong et al., 2002). Briefly, a homology arm corresponding to the region immediately upstream of the ATG translation initiation site of the *Abcb1a* gene was cloned into the pS296 targeting vector (Heiman et al., 2008) containing EGFPL10a using the *AscI* and *NotI* restriction sites. Recombination was performed by electroporating the pS296-Abcb1a vector into electrocompetent DH10 β bacteria containing pSV1.RecA plasmid and the BAC. Successful recombination was determined by screening cointegrates by PCR and Southern blot analysis of *HindIII* digested BAC DNA, using the homology region as a probe. The modified BAC was prepared by double acetate purification with CsCl centrifugation followed by membrane dialysis and microinjected into the pronuclei of fertilized FVB/N mouse oocytes at a concentration of 0.5 ng/ μ l. Six transgenic founder mice were generated and crossed to C57BL/6J mice. F1 progeny were screened for proper transgene expression by EGFP immunohistochemistry. Founder line ES3026 showed accurate and robust expression of the transgene and was therefore selected for colony expansion.

Generation of AAVs

The plasmid pAAV-FLEX-EGFPL10a was generated in an analogous fashion to pAAV-FLEX-NBL10 (Ekstrand et al., 2014). Briefly, the EGFPL10a transgene was PCR amplified from the pS296 targeting vector (Heiman et al., 2008) adding 5' NheI and 3' AscI restriction sites. The amplicon was then subcloned into pAAV-EF1a-DIO-hChR2 (H134R)-mCherry-WPRE-HGHpA (Addgene plasmid #20297) in the reverse orientation using NheI and AscI sites, replacing ChR2-mCherry, to create pAAV-FLEX-EGFPL10a. Plasmids were then packaged into AAVs serotyped with AAV5 capsids at the University of North Carolina Vector Core or AAV2 and AAV9 capsids at the University of Pennsylvania Vector Core. Virus titers were 1.63×10^{13} gc/ml for AAV5, 4.7×10^{12} gc/ml for AAV2, and 7.47×10^{12} gc/ml for AAV9.

Stereotaxic Surgeries

Surgeries were performed on adult mice (8-20 weeks old) under ketamine/xylazine (100/10 mg/kg) anesthesia. Single bilateral stereotaxic injections of 0.25-1.0 μ l pAAV-FLEX-EGFPL10a were done using the following injection sites: DRN, +0.8 mm ML, 0 mm AP from lambda, -3.0 mm DV from dura, injected at a 15° angle; VTA \pm 1.0 ML, -3.15 AP from bregma, -4.23 DV from dura, injected at a 7° angle; LH \pm 1.56 ML, -1.2 AP from bregma, -4.75 DV, injected at a 8° angle; S1BF, \pm 2.5 ML, -1.0 AP from bregma, -0.75 DV from dura. For S1BF injections, a single bilateral injection of 0.25 μ l virus into S1BF was done for each serotype. Following injections, the needle was slowly retracted and skin was closed with a surgical clip. Animals were sacrificed 3-4 weeks after surgery and tissue was collected for polysome immunoprecipitations or immunohistology as described. For polysome fractionation experiments, 0.3 μ l AAV9 pseudotyped pAAV-FLEX-EGFPL10a virus was bilaterally injected into S1BF at three sites spaced 0.2 mm apart in the AP plane of Emx1-Cre mice. Mice were sacrificed for polysome biochemistry either one week or four weeks after surgery (see below).

Immunohistochemistry

Mice were deeply anesthetized and transcardially perfused with PBS followed by 4% paraformaldehyde in PBS. Brains were dissected and postfixed for 8-12 hours at 4°C, cryopreserved in 30% sucrose solution, and sectioned on a freezing microtome (35 μ m sections). Free-floating sections were immunofluorescently stained with chicken anti-GFP (1:2000, Abcam, Cambridge, MA, Cat# ab13970), mouse anti-NeuN (1:1000, Millipore, Billerica, MA, Cat# MAB377B), anti-TH (1:1000, Pel-Freez, Rogers, AR), anti-TPH2 (1:500, Novus Biologicals, Littleton, CO, Cat# NB100-74555), and anti-MCH (1:1000, Phoenix Pharmaceuticals, Burlingame, CA) primary antibodies. Sections were blocked for 60 min in PBS containing 2.5% normal goat serum (NGS) and 0.1% Triton-X-100 and then incubated overnight at 4°C with primary antibodies diluted in PBS containing 11% NGS and 0.1% Triton-X-100. Sections were washed with PBS and incubated for one hour at room temperature with Alexa-fluor conjugated secondary antibodies (Life Technologies, Waltham, MA) diluted in PBS. All sections were imaged on either a Zeiss LSM780 or LSM700 confocal microscope.

For cell culture experiments, HEK293T cells were co-transfected with pAAV-FLEX-EGFPL10a and pCAG-Cre (Addgene plasmid #13775) using the Fugene-6 transfection method (Roche Diagnostics, Indianapolis, IN). After 36 hours, cells were fixed with 4% paraformaldehyde in PBS and visualized by immunofluorescent staining with chicken anti-GFP (as above) and mouse anti-c-Myc clone 9E10 (1:1000, Sigma-Aldrich, St. Louis, MO, Cat# M5546) primary antibodies followed by Alexa Fluor-488-conjugated goat anti-chicken and Alexa Fluor-568-conjugated goat anti-mouse secondary antibodies. Cells were then coverslipped and imaged on a Zeiss LSM700 confocal microscope.

Translating ribosome affinity purification

Affinity purification of EGFP-tagged polysomes was carried out as previously described (Heiman et al., 2014). IPs were done 3-4 weeks after viral injections and three biological replicates consisting of brain tissue pooled from 3-5 mice (male and female) were used for each condition. Mice were sacrificed, followed by rapid dissection of brain tissue in ice-cold HBSS containing 2.5 mM HEPES-KOH (pH 7.4), 35 mM glucose, 4 mM NaHCO₃, and 100 µg/ml cycloheximide. Tissue containing relevant brain regions (e.g. whole cortex, hypothalamus) was then homogenized in extraction buffer containing 10 mM HEPES-KOH (pH 7.4), 150 mM KCl, 5 mM MgCl₂, 0.5 mM DTT, 100 µg/ml cycloheximide, RNasin (Promega, Madison, WI) and SUPERas-In™ (Life Technologies) RNase inhibitors, and Complete-EDTA-free protease inhibitors (Roche), and then cleared by centrifugation at 2000 x g. IGEPAL CA-630 (NP-40, Sigma) and DHPC (Avanti Polar Lipids, Alabaster, AL) were both added to the S2 supernatant to a final concentration of 1% for each, followed by centrifugation at 20,000 x g. Polysomes were immunoprecipitated from the S20 supernatant using 100 µg monoclonal anti-EGFP antibodies (50 µg each of clones 19C8 and 19F7; see Heiman et al., 2008) bound to biotinylated-Protein L (Pierce, Thermo Fisher, Waltham, MA) coated streptavidin-conjugated magnetic beads (Life Technologies), and washed in high salt buffer containing 10 mM HEPES-KOH (pH7.4), 350 mM KCl, 5 mM MgCl₂, 1% IGEPAL CA-630, 0.5 mM DTT, 100 µg/ml cycloheximide, and RNasin RNase inhibitors (Promega). IPs were carried out overnight at 4°C. Bound RNA was purified using the Absolutely RNA Nanoprep kit (Agilent, Santa Clara, CA). RNA was also purified from a fraction of the pre-IP S20 supernatant to serve as whole-tissue “input” samples. RNA quantity was measured with a Nanodrop 1000 spectrophotometer and quality was assayed on an Agilent 2100 Bioanalyzer. Only samples with RNA integrity values >7.0 were used for RNA-seq and qRT-PCR analyses.

RNA-seq

For cortical samples, 15 ng of total RNA was amplified using the Ovation RNA-Seq System V2 Kit (NuGEN, San Carlos, CA) and RNA-seq libraries were prepared from 10 µg amplified RNA using the TruSeq RNA Sample Preparation Kit v2 (Illumina, San Diego, CA) following manufacturer’s protocols. MCH neuron RNA-seq libraries were prepared with oligo-dT priming using the SMARTer Ultra Low RNA Kit (Clontech, Mountain View, CA). Sequencing reactions (50 b.p., single end for all Ntsr1 samples, and 100 b.p., single end for MCH samples) were done using the Illumina HiSeq 2500 platform with three samples multiplexed per sequencing lane. RNA-seq read quality was assessed with FASTX Toolkit 0.0.13 and sequences were trimmed for trailing adaptors. Trimmed reads were then aligned to annotated exons using the mm10 mouse reference genome with STAR (Dobin et al., 2013) version 2.0.0e_r291 using default settings. The numbers of raw and mapped reads for each sample are presented in the table “Quality Control of RNA-seq Alignments” below. Quantification of aligned reads was done using the htseq-count module of the HTSeq framework (Anders et al., 2015) version 0.6.0 using the “union” mode with default settings to generate raw counts for each sample. Differential expression was calculated by DESeq2 (Love et al., 2014) version 1.4.5 using default settings and filtering for an FDR cutoff of <0.05 and |log₂| fold change >1.0. For scatter plots (Figures 3D, 4B, 5C, 6A, and S5B), data are displayed as log₂ mean of raw counts normalized to sample size for each sample (“normalized counts”) as calculated by DESeq2. For specificity index analysis of multiple distinct cell types, cell specific gene expression quantification was carried out on DESeq2 normalized TRAP-seq counts using the pSI (Specificity Index Statistic) R-package version 1.1 (Dougherty et al., 2010). For Figures 3C and E, RNA-seq data were normalized as fragments per kilobase of transcript per million mapped reads (FPKM) using Cufflinks v2.1.1. Fold-enrichment was calculated as FPKM of GFP IP divided by FPKM Input (IP/Input). RPKMs in Figure S5C and D were calculated as: RPKM = (10⁹ * Count)/(Library Size * Gene Length), with Gene Length being the maximum sum of annotated exon lengths of gene transcripts for a given gene (based on GENCODE VM9 [Ensembl 84], updated March 14, 2016). RNA-seq data sets have been deposited in NCBI’s Gene Expression Omnibus (GEO; Barret et al., 2013), and are accessible through GEO Series accession number GSE89737.

For comparison of vTRAP to single cell RNA-seq results in Figure S5, raw sequence read archives (SRAs) of published single cell RNA-seq data were downloaded from NCBI’s GEO. Data sets from GEO: GSE71585 representing six individual “Core” cells from Primary Type Cells “L6a Sla” (Cell ID T02251526, GEO: GSM1839921; T01101413, GEO: GSM1839898; T02271422, GEO: GSM1839927; T01101411, GEO: GSM1839896; T07011417, GEO: GSM1839960; and T07011415, GEO: GSM1839958) and “L6a Mgp” (T07011423, GEO: GSM1839966; T05151410, GEO: GSM1839939; T05151405, GEO: GSM1839934; T02251501, GEO: GSM1839902; T01101410, GEO: GSM1839895; T02271423, GEO: GSM1839928) were randomly selected for analysis (Tasic et al., 2016). Six data sets from GEO: GSE60361 representing “S1Pyr6” cells (Zeisel et al., 2015) were selected based on their expression of the cell-type markers *Rprm*, *Foxp2*, and *Syt6* (1772071041_E04, GEO: GSM1477180; 1772071040_F06, GEO: GSM1477141; 1772067073_G04, GEO: GSM1476683; 1772067074_C04, GEO: GSM1476697; 1772067074_G06, GEO: GSM1476721; 1772067064_A11, GEO: GSM1476528). All raw sequencing data sets were processed as described above.

Quality Control of RNA-seq Alignments.

Sample	Raw Reads	Uniquely Mapped Reads	% Uniquely Mapped Reads	% Aligned Bases Mapped to mRNA*
Ntsr1 bacTRAP IP rep 1	72,542,951	56,327,123	77.65	70.7724
Ntsr1 bacTRAP IP rep 2	69,360,209	54,582,713	78.69	74.2391
Ntsr1 AAV2 IP rep 1	67,797,151	53,303,721	78.62	74.5542

Ntsr1 AAV2 IP rep 2	57,147,662	45,017,131	78.77	75.054
Ntsr1 AAV2 IP rep 3	60,796,930	47,765,900	78.57	74.9366
Ntsr1 AAV5 IP rep 1	58,284,352	44,636,629	76.58	75.2089
Ntsr1 AAV5 IP rep 2	48,031,599	36,300,939	75.58	73.9679
Ntsr1 AAV5 IP rep 3	47,091,409	36,381,832	77.26	75.8054
Ntsr1 AAV9 IP rep 1	77,836,295	57,217,810	73.51	67.0368
Ntsr1 AAV9 IP rep 2	73,561,919	55,719,055	75.74	64.402
Ntsr1 AAV9 IP rep 3	79,455,352	62,665,474	78.87	68.0555
bacTRAP cortex input rep 1	117,570,640	96,792,310	82.33	63.4668
bacTRAP cortex input rep 2	127,417,769	101,738,934	79.85	63.5548
AAV2 cortex input rep 1	60,589,103	48,242,443	79.62	61.043
AAV2 cortex input rep 2	58,975,851	46,766,108	79.30	59.2499
AAV2 cortex input rep 3	67,119,968	52,608,978	78.38	61.3017
AAV5 cortex input rep 1	52,801,324	42,071,998	79.68	58.3502
AAV5 cortex input rep 2	56,330,442	44,226,435	78.51	54.0793
AAV5 cortex input rep 3	53,762,949	42,248,320	78.58	62.3024
AAV9 cortex input rep 1	78,811,731	62,506,741	79.31	58.4366
AAV9 cortex input rep 2	75,437,329	59,829,050	79.31	59.0644
AAV9 cortex input rep 3	77,435,616	62,244,294	80.38	61.1087
MCH IP rep 1	30,125,935	25,759,835	85.51	84.3355
MCH IP rep 2	32,654,548	27,928,690	85.53	77.4527
MCH IP rep 3	29,552,843	25,254,467	85.46	85.0989
MCH input rep 1	35,197,999	30,080,429	85.46	77.2914
MCH input rep 2	21,227,735	17,419,466	82.06	83.1531
MCH input rep 3	29,554,526	24,778,076	82.84	75.8473

*These are the percentage of total bases mapping to Coding + UTRs.

Polysome fractionation

Polysome fractionations were collected by centrifugation in a sucrose gradient as described previously(Darnell et al., 2011). Briefly, mice were sacrificed one or four weeks after AAV injection and cortices were rapidly dissected in ice-cold HBSS containing 2.5 mM HEPES-KOH (pH 7.4), 35 mM glucose, 4 mM NaHCO₃, and 100 µg/ml cycloheximide. Each cortex (two hemispheres) was homogenized in 1 ml gradient buffer containing 20 mM HEPES-KOH (pH 7.4), 150 mM NaCl, 5 mM MgCl₂, 0.5 mM DTT, 100 µg/ml cycloheximide, RNasin RNase inhibitors (Promega), and Complete-EDTA-free protease inhibitors (Roche), and then cleared by centrifugation at 2000 x g at 4°C. IGEPAL CA-630 (NP-40, Sigma) was added to the S2 supernatant to a final concentration of 1% followed by centrifugation at 20,000 x g at 4°C. The S20 supernatant was then loaded onto a 20%–50% w/w linear density gradients of sucrose in 10mM HEPES-KOH, pH 7.4, 150mM NaCl, 5mM MgCl₂ and centrifuged at 40,000 r.p.m. for 2 hr at 4°C in a Beckman Instruments (Fullerton, CA) SW41 rotor. Fractions of 0.69 ml volume were collected with continuous monitoring at 254 nm using an ISCO UA-6 UV detector (ISCO, Inc, Lincoln, NE). TCA-precipitated proteins from 200 µl of each fraction were analyzed by Western blot, separated on 8% tris-glycine polyacrylamide gels (Novex, Thermo Fisher) and transferred to Optitran BA-S83 membranes (Whatman, Sigma-Aldrich) by standard methods. Membranes were blocked for 1hr at room temperature in 5% non-fat dry milk (Carnation) in PBS followed by addition of primary antibody for 1 hr at room temperature or overnight at 4 degrees. Blots were washed 4 X 5 min with Western blot wash buffer (23mM Tris, pH 8.0, 190mM NaCl, 0.1% w/v BSA, 1 mM EDTA, 0.5% Triton X-100, 0.02% SDS) after each antibody incubation. HRP-conjugated secondary antibodies (Jackson Immuno Research, West Grove, PA) were used at 1:10,000 in 5% milk/PBS for 1 hr at RT, blots were washed as before, and HRP signal was detected by enhanced chemiluminescence (Western Lightning Plus detection kit, Perkin Elmer, Waltham, MA) followed by quantification by densitometry of scanned films (Kodak MR film, ImageJ software). Primary antibodies were anti-RPL10a mouse monoclonal antibody (M01), clone 3G2 (Abnova Corporation, Walnut, CA, Cat# H00004736-M01) at 1:1,000; anti-GFP mouse monoclonal (B-2; Santa Cruz Biotechnology, Dallas, TX, Cat# sc-9996) at 1:200; and anti-RPS6 rabbit monoclonal antibody (5G10; Cell Signaling Technology, Danvers, MA,Cat# 2217).

Quantitative RT-PCR

qRT-PCR was performed on either an Applied Biosystems 7500 Fast or StepOnePlus Fast Real-Time PCR System using Taqman assays (see table below titled “TaqMan Gene Expression Assays used for qPCR”) and following standard cycling conditions (50°C for

2 min, 95°C for 10 min, then 40 cycles of 95°C for 15 s and 60°C for 1 min). Ten nanograms of cDNA prepared independently from the RNA-seq libraries were used for each qRT-PCR reaction and technical triplicates were run for three biological replicates for each condition. The mean C_T for technical replicates was used for quantification. For Figures 2C, 3B and S2, data are normalized to *Rpl23* expression by standard curve. For Figures 4D and 6G, data are normalized to *Actb* by the comparative C_T ($2^{-\Delta\Delta CT}$) method (Livak and Schmittgen, 2001). Data are presented as mean ± SEM of biological triplicates.

TaqMan Gene Expression Assays used for qPCR.

Symbol	Gene Name	Source	Assay	Dye
<i>Actb</i>	actin, beta	Life Technol.	Mm00607939_s1	FAM
<i>Agrp</i>	agouti-related peptide	IDT DNA	Mm.PT.56a.31030782.gs	FAM
<i>Anxa1</i>	annexin A1	IDT DNA	Mm.PT.58.12626377	FAM
<i>Cartpt</i>	cocaine- and amphetamine-regulated transcript	IDT DNA	N001081493.1.pt.Cartpt	FAM
<i>Cbln1</i>	cerebellin 1 precursor protein	Life Technol.	Mm01247194_g1	FAM
<i>Cbln4</i>	cerebellin 4 precursor protein	Life Technol.	Mm01249788_m1	FAM
<i>Cldn1</i>	claudin 1	Life Technol.	Mm00516701_m1	FAM
<i>Crhbp</i>	corticotropin releasing hormone binding protein	IDT DNA	Mm.PT.56a.8159672	FAM
<i>Dmrtb1</i>	dmrt-like family B with proline-rich c-terminal, 1	IDT DNA	Mm.PT.58.43084043	FAM
<i>Fev</i>	fev (ets oncogene family)	IDT DNA	Mm.PT.56a.8125305	FAM
<i>Foxp2</i>	forkhead box P2	Life Technol.	Mm00475030_m1	FAM
<i>Mal</i>	myelin and lymphocyte protein, T cell differentiation protein	Life Technol.	Mm01339780_m1	FAM
<i>Mup6</i>	major urinary protein 6	IDT DNA	Mm.PT.58.42371435	FAM
<i>Nnat</i>	neuronatin	Life Technol.	Mm00731416_s1	FAM
<i>Ntsr1</i>	neurotensin receptor 1	Life Technol.	Mm00444459_m1	FAM
<i>Pmch</i>	pro-melanin concentrating hormone	IDT DNA	N029971.1.pt.Pmch	FAM
<i>Pth2r</i>	parathyroid hormone 2 receptor	Life Technol.	Mm00653029_m1	FAM
<i>Rpl23</i>	ribosomal protein L23	IDT DNA	Mm.PT.56a.10484606.g	FAM
<i>Slc6a3</i>	dopamine transporter		Homemade assay	FAM
<i>Slc6a4</i>	serotonin transporter	IDT DNA	Mm.PT.56a.43910045	FAM
<i>Slc32a1</i>	vesicular GABA transporter	IDT DNA	Mm.PT.58.6658400	FAM
<i>Syt6</i>	synaptotagmin VI	Life Technol.	Mm01308768_m1	FAM
<i>Tacr3</i>	tachykinin 3 receptor	IDT DNA	Mm.PT.42.6434400	FAM
<i>Th</i>	tyrosine hydroxylase		Homemade assay	FAM
<i>Tmem200a</i>	transmembrane protein 200A	Life Technol.	Mm01190399_m1	FAM

Scoring Allen Mouse Brain Atlas *in situ* hybridizations

The expression pattern of “bacTRAP-specific” and “vTRAP-specific” genes was qualitatively scored by a blinded observer using the Allen Mouse Brain Atlas ISH database for adult mouse brain (Lein et al., 2007). All scores were done using sagittal data sets since this orientation is available for all genes in the database. When available, coronal data sets were used to confirm the score since this orientation provides the most direct assessment of laminar and areal subdivisions of cortex. A gene was scored as “Regional” if there had distinct ISH signal (at least two color levels above values of neighboring areas of cortex in the ABA “expression viewer”) in layer 6 of the neocortex in rostral and/or caudal regions that did not overlap with the AAV injection site (green ovals in Figure 6C), or expression was restricted to the AAV injection site and not found at rostral or caudal regions. Genes widely absent from the neocortex but with distinct ISH signal in entorhinal cortex were also scored as “Regional” due to entorhinal cortex labeling in the Ntsr1-bacTRAP (TS16) mouse line. Additionally, genes were scored as “Widespread” if expression was distributed throughout the rostral-caudal plane of layer 6 of the neocortex, or seen in layer 6 as well as other layers, “No Signal” if the ISH had no detectable signal anywhere in the brain or was of low quality (no signal above the lowest color level in the “expression viewer”), “Not Expressed” if there was no expression within layer 6 of neocortex (but clear expression elsewhere), or “No Data” if the gene was not found in the data base.

Statistics

All data analysis was performed in Graphpad Prism, Microsoft Excel, or R (R Core Team, 2013). Student's t-test was used to compare differences in qRT-PCR results between IP and input samples in Figures 2D, 3F, 4D, and 6G. Two-way ANOVA on the log₂ fold change values was used to compare each of the vTRAP groups against bacTRAP for the specified genes in Figures 4D and 6G. Statistical methods used to analyze RNA-seq data are discussed in the "RNA-seq" section.

SUPPLEMENTAL REFERENCES

- Barrett T, Wilhite SE, Ledoux P, Evangelista C, Kim IF, Tomashevsky M, Marshall KA, Phillippy KH, Sherman PM, Holko M, Yefanov A, Lee H, Zhang N, Robertson CL, Serova N, Davis S, Soboleva A. (2013). NCBI GEO: archive for functional genomics data sets--update. *Nucleic Acids Res* 41, D991-5. 10.1093/nar/gks1193
- Gong, S., Kus, L., and Heintz, N. (2010). Rapid bacterial artificial chromosome modification for large-scale mouse transgenesis. *Nat Protoc* 5, 1678-1696. 10.1038/nprot.2010.131
- Gong, S., Zheng, C., Doughty, M.L., Losos, K., Didkovsky, N., Schambra, U.B., Nowak, N.J., Joyner, A., Leblanc, G., Hatten, M.E., et al. (2003). A gene expression atlas of the central nervous system based on bacterial artificial chromosomes. *Nature* 425, 917-925.
- Gong, S., Yang, X.W., Li, C., and Heintz, N. (2002). Highly efficient modification of bacterial artificial chromosomes (BACs) using novel shuttle vectors containing the R6Kgamma origin of replication. *Genome Res* 12, 1992-1998.